Journal of
Water & Climate Change

IWA PUBLISHING

Journal of Water and Climate Change Vol 14 No 2, 494 doi: 10.2166/wcc.2023.352

Projections and impact assessment of the local climate change conditions of the Black Volta Basin of Ghana based on the Statistical DownScaling Model

Ebenezer K. Siabi [a,b,*], Dang Nguyen Dong Phuong [c], Amos T. Kabobah [d], Komlavi Akpoti [e], Geophery Anornu [f], Awo Boatemaa Manson Incoom [g], Emmanuel Kwesi Nyantakyi[h], Kofi Antwi Yeboah[h], Sarah Elikplim Siabi [h], Christopher Vuu [f], Martin Kyere Domfeh [a], Eric Mensah Mortey [a], Cosmos Senyo Wemegah [a], Francis Kudjoe [a], Precious Dapaah Opoku [a], Austin Asare [i], Samuel Kofi Mensah[h], Peter Donkor[j], Emmanuel K. Opoku[f], Zié Adama Ouattara[b], Nana Kwame Obeng-Ahenkora[h], Daniel Adusu [i] and Andrew Quansah[k]

[a] Earth Observation Research and Innovation Center (EORIC), University of Energy and Natural Resources, P.O. Box 214, Sunyani, Ghana
[b] Regional Center for Energy and Environmental Sustainability, University of Energy and Natural Resources, P.O. Box 214, Sunyani, Ghana
[c] Research Center for Climate Change, Nong Lam University Ho Chi Minh City, Ho Chi Minh City 700000, Vietnam
[d] International Relations Office, University of Energy and Natural Resources, P.O. Box 214, Sunyani, Ghana
[e] International Water Management Institute (IWMI), Accra, Ghana
[f] Regional Water and Environmental Sanitation Centre, Kumasi (RWESCK), Kwame Nkrumah University of Science and Technology, Kumasi, Ghana
[g] Department of Fisheries and Water Resources, University of Energy and Natural Resources, P.O. Box 214, Sunyani, Ghana
[h] Department of Civil and Environmental Engineering, University of Energy and Natural Resources, P.O. Box 214, Sunyani, Ghana
[i] Department of Environmental Management, University of Energy and Natural Resources, P.O. Box 214, Sunyani, Ghana
[j] School of Public Service and Governance, Ghana Institute of Management and Public Administration, P.O. Box AH50, Achimota, Accra, Ghana
[k] Department of Computer and Electrical Engineering, UENR, P.O. Box 214, Sunyani, Ghana
*Corresponding author. E-mail: siabikebenezer@gmail.com; ebenezer.siabi@uenr.edu.gh

EKS, 0000-0001-8563-6689; DNDP, 0000-0001-8881-5105; ATK, 0000-0002-1361-4250; KA, 0000-0001-6435-5116; GA, 0000-0003-3691-5635; ABMI, 0000-0003-1181-4125; SES, 0000-0002-5300-7156; CV, 0000-0003-2766-5080; MKD, 0000-0001-6612-7301; EMM, 0000-0003-2199-7340; CSW, 0000-0002-5936-0268; FK, 0000-0002-9489-218X; PDO, 0000-0001-7910-8185; AA, 0000-0003-4979-1416; DA, 0000-0003-2994-2846

ABSTRACT

The uncertainties and biases associated with Global Climate Models (GCMs) ascend from global to regional and local scales which delimits the applicability and suitability of GCMs in site-specific impact assessment research. The study downscaled two GCMs to evaluate effects of climate change (CC) in the Black Volta Basin (BVB) using Statistical DownScaling Model (SDSM) and 40-year ground station data. The study employed Taylor diagrams, dimensionless, dimensioned, and goodness of fit statistics to evaluate model performance. SDSM produced good performance in downscaling daily precipitation, maximum and minimum temperature in the basin. Future projections of precipitation by HadCM3 and CanESM2 indicated decreasing trend as revealed by the delta statistics and ITA plots. Both models projected near- to far-future increases in temperature and decreases in precipitation by 2.05-23.89, 5.41–46.35, and 5.84–35.33% in the near, mid, and far future respectively. Therefore, BVB is expected to become hotter and drier by 2100. As such, climate actions to combat detrimental effects on the BVB must be revamped since the basin hosts one of the largest hydropower dams in Ghana. The study is expected to support the integration of CC mitigation into local, national, and international policies, and support knowledge and capacity building to meet CC challenges.

Key words: Black Volta Basin, climate change, GCMs, impact assessment, Innovative-Sen Trend Analysis, SDSM

HIGHLIGHTS

- The study downscaled two GCMs to evaluate the effects of climate change over the Black Volta Basin using the SDSM.
- The study revealed that the SDSM provided a good performance across the selected stations.
- Both models projected near-to-future decreases in precipitation in the near-, mid-, and far-future.
- The Black Volta Basin is expected to become hotter and drier by 2100.
- The SDSM is a powerful tool for climate change assessment.

GRAPHICAL ABSTRACT

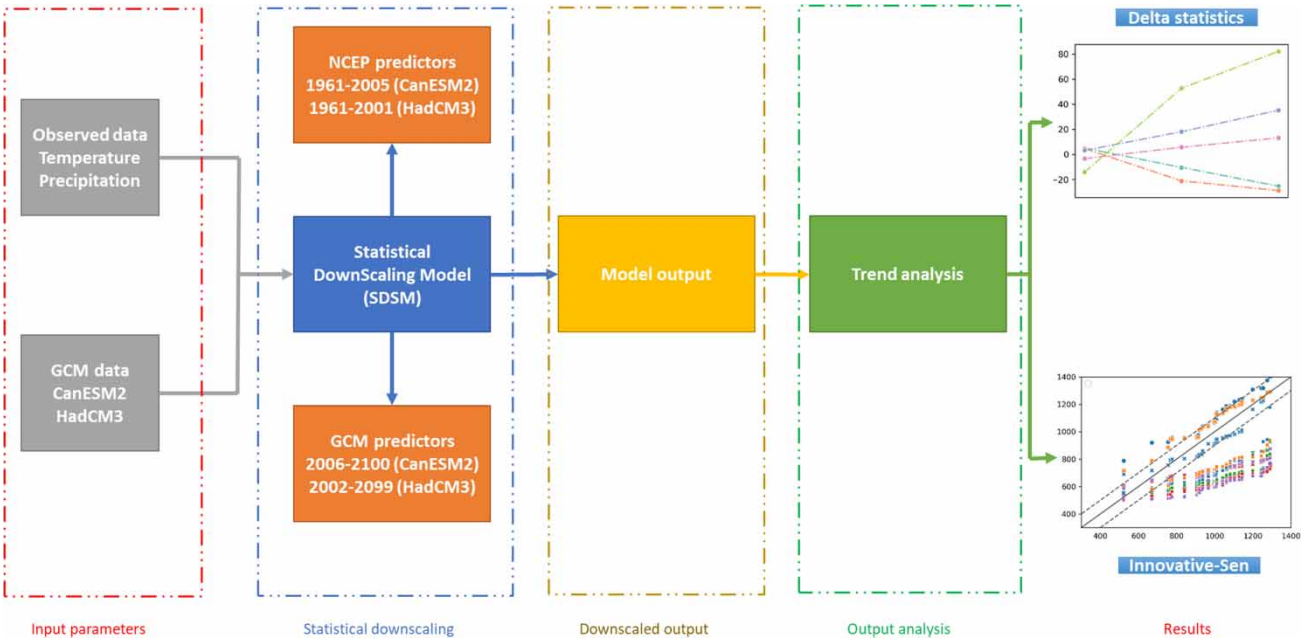

1. INTRODUCTION

Global or large-scale Climate Models (GCMs) are presently employed in the development of scientific understanding and knowledge of climate change and variabilities in large-scale climate data (Dixon *et al.* 2016). Data acquired from GCMs provide in-depth comprehension of the present and future climate at a holistic scale (IPCC 2007, 2014). The >100-km resolution of GCM outputs renders them too coarse to be utilized in impact studies, decision-making processes, and adaptation planning at a local or regional scale (Meenu *et al.* 2013). Additionally, the limitations on the applicability and usefulness of GCMs in site-specific impact assessment studies are caused by the uncertainties and biases associated with GCMs that increase from global to regional to local scales (Lutz *et al.* 2016). Therefore, downscaling is required to increase the spatial resolution, reduce bias, and help accelerate climate forecasts for impact analysis and adaptation strategy. Presently, there are two types of downscaling techniques available to reduce biases and improve the spatial resolution of GCMs. These include statistical and dynamic downscaling techniques. The dynamic downscaling such as CORDEX (http://www.cordex.org/domains/region-5-africa/) contains local data which comprises topographic components that produce a high-resolution climate forecasting, for instance, 50 km for Africa (Dosio & Panitz 2016). One disadvantage of the dynamic downscaling process is its high computational resource requirements. Therefore, these models have inherent sensitivity and biases to the precinct of GCMs, and this limits their utilization in impact assessment and adaptation studies at the local scale (Wilby & Dawson 2007). Relatively, statistical downscaling models are simple, efficient, and fast which require low computational powers and expenses.

Statistical models are built to offer site-specific weather series that are equivalent to station data through the development of statistical relationships between large-scale climate variables also known as predictors and site-specific climate variables known as predictands. The advantages of the statistical downscaling techniques are that they are extensively employed in impact studies such as water and agriculture at the regional and local scale (Wilby & Dawson 2007; Tavakol-Davani *et al.* 2013). Generally, statistical models are categorized under three classes premised on the statistical approach; weather typing (Anandhi *et al.* 2011), weather generator (Semenov & Barrow 1997), and transfer function (Wilby & Dawson 2007).

The Statistical DownScaling Model (SDSM) (Wilby & Dawson 2007) is among the extensively applied statistical downscaling models that are built premised on a transfer function and stochastic weather generator (Hassan *et al.* 2013). Furthermore, the SDSM was found to be better than conventional weather generators in terms of performance (Mohorji *et al.* 2017) especially in capturing precipitation (Prcp), minimum (T_{min}), and maximum (T_{min}) temperature (Wilby & Dawson 2007; Hassan *et al.* 2013). Therefore, the SDSM is employed to simulate station-specific high-resolution climate projections for

the Black Volta Basin (BVB). Most regions in Africa, especially in West Africa, are highly susceptible to changes in climate extremes such as weighty rainstorms, droughts, and frequent inundations and will be more severe considering future projections (Gebrechorkos *et al.* 2019a). To contemplate the observed susceptibility and changes of the BVB to variability (for instance precipitation variability) and changes in climate and extremes (Gebrechorkos *et al.* 2019a), undertaking a detailed impact study on the local scale is required to reduce or mitigate the effects in the forthcoming years via sustainable adaptation procedures. However, this category of data is scarce, and attaining site-specific climate projections using the SDSM needs high-resolution observed data for calibration and validation, as well as the ensemble of synthetic weather series employing daily GCM predictors (Wilby & Dawson 2007).

Observed weather ground station data in Ghana is generally limited due largely to issues such as limited spatial and temporal, accessibility (data distribution policies), and data quality. As a result, the dataset used was significantly influenced by the availability and consistency of the data collected. This, therefore, influenced the selection of the stations used in the study.

The application of the SDSM has been widely established throughout the world over the last decade for future climate change assessment at local scale. For instance, previous studies (Liu *et al.* 2011; Tryhorn & Degaetano 2011; Campozano *et al.* 2016) compared the performance of the SDSM to other models such as the Markov model, artificial neural networks, and least square support vector machine. Liu *et al.* (2011) found that the SDSM performed well in simulating the inter-site correlation features of the weather stations compared to the Markov model which simulated the multi-site prediction. Moreover, while assessing the extreme precipitation over the northern United States (Tryhorn & Degaetano 2011), it was found that the SDSM is capable of matching observed extreme climatology well compared to spatial disaggregation, and bias correction. Furthermore, Campozano *et al.* (2016) revealed that the SDSM is capable of simulating the median and variance of the depths of the monthly ground station data better than the artificial neural networks and least square support vector machine.

In Africa, a few studies (Wilby *et al.* 2014; Gulacha & Mulungu 2016; Matthew *et al.* 2017; Gebrechorkos *et al.* 2019a; Iwadra 2019) have successfully applied the SDSM with good performances. For example, Gebrechorkos *et al.* (2019a) found that the SDSM recorded good performance (>80, 79, and 96%) during validation for precipitation, minimum, and maximum temperature, respectively, in East Africa. Gulacha & Mulungu (2016) also found the performance of the SDSM ranging from 21–63% for precipitation and 60–98% for temperature in the Wami-Ruvu river basin in Tanzania. Again, the findings of Iwadra (2019) revealed the performance of the SDSM between 75–85% in the Aswa catchment of Uganda.

Currently, there is little or no study on the application of the SDSM in Ghana, especially in the BVB. Majority of the studies (Matthew *et al.* 2017; Osei *et al.* 2019; Awotwi *et al.* 2021; Sekyi-annan *et al.* 2021) conducted in Ghana applied the CMHyd model to bias-correct the hydro-climatic variables, especially under the Representative Concentration Pathway (RCP) scenarios. Studies on the A2 and B2 scenarios are still lacking in the BVB. Although these are old scenarios, their importance in future decision-making cannot be overlooked. It is worth noting that these studies coupled the CMHyd model with other hydrological and hydraulic tools such as the Soil Water Analysis Tool (SWAT), MIKE, HEC-HMS, etc., necessitates historical and future data as tangible inputs for the assessment of the impacts of climate change on hydrological resources at the basin scale. The BVB hosts one of Ghana's hydropower dams which provides 400 MW of power to the electricity grid in Ghana. Furthermore, the BVB extends over productive agricultural lands whose predominant activities are extensively rainfed and livestock farming. The past and future impacts of climate variabilities and changes on water availability in the BVB have been established in previous studies (Akpoti *et al.* 2016; Kabo-Bah *et al.* 2016).

Therefore, the main objective of this study is to calibrate and validate the analog technique as a method to downscale daily precipitation (Prcp), minimum (T_{min}), and maximum (T_{max}) temperature for specific stations of a data-scarce basin such as the BVB. This is critical to driving impact assessment models to evaluate the impact of future climate changes on sectors such as agriculture, hydrology, and urbanization in the basin which addresses the sustainable development goals 11 and 13 (UN 2023). In this study, future climate changes were downscaled under multiple climate scenarios based on three climatic periods 2011–2039, 2040–2069, and 2070–2099 as 2020s, 2050s, and 2080s, respectively. The outputs presented in the Innovative Trend Analysis (ITA) will assist in the identification of future climate trends in a detailed manner that could support the development of sustainable mitigation and adaptation strategies in the basin based on the climatic periods.

1.1. The A2, B2, RCPs 2.6, 4.5, and 8.5 climate scenarios

The A2 climate scenario describes a world of self-dependence and securing local identities. Thus, where countries operate independently, under this scenario, there is a slow convergence of the patterns of fertility across regions. This results in a

rapidly high population. Also, there is an expansion in economies, per capita, and technologies. However, these expansions are regionally centered leaving them more fragmented than other narratives (IPCC 2007).

However, under the B2 climate scenario, the world tends to focus on local solutions to tackle environmental, economic, and social sustainability. Population under this scenario is expected to increase, however, at a lower rate compared to the A2 climate scenario. Similarly, there is an expected increase in economic development but at intermediate levels. This is expected to be fairly rapid, however, expansions in technologies are expected to be more heterogeneous by the end of the 21st century. Despite this scenario being social equity and environmental safety oriented, it focuses on local and regional levels more than the other narratives. This results in varying global warming under these scenarios.

For the Coupled Model Intercomparison Project 5 (CMIP5) under the RCPs, there are three different climate scenarios ranging from RCP 2.6 (the scenario where there is low emission as a result of active mitigation), RCPs 4.5 and 6.0 (the intermediate scenarios) as well as the RCP 8.5 (worst-case scenario/high ended emission scenario). Furthermore, the RCP scenarios have probable combinations of expected high population, energy intensity, and socio-economic development. The naming of the RCP scenarios follows their total radiative forcing by/or post 2100. For instance, under the RCP 2.6, the radiative forcing is expected to peak at approximately 3 W/m^2 in the mid-century before dropping to 2.6 W/m^2 by 2100, whereas the radiative forcing is expected to plateau without spiking at 4.5 W/m^2 by/post-2100 under the RCP 4.5 and rise to 8.5 W/m^2 by 2100 under RCP 8.5 (van Vuuren *et al.* 2011).

2. MATERIALS AND METHODS

2.1. Study area description

Geographically, the BVB is located between latitude and longitude 7°00′00″N and 14° 30′00″N and 5°30′00″ W and 1° 30′ 00″ W, respectively (Figure 1). The basin has an entire land area of about 130, 400 km^2 representing 21% of the total Volta basin (Smit & Wandel 2006). However, the portion of the basin in Ghana covers about 18,384 km^2. This represents about 14% of the total area of the Volta basin (Smit & Wandel 2006). The BVB encompasses two and three districts in Ghana, Burkina Faso, Cote d'Ivoire,

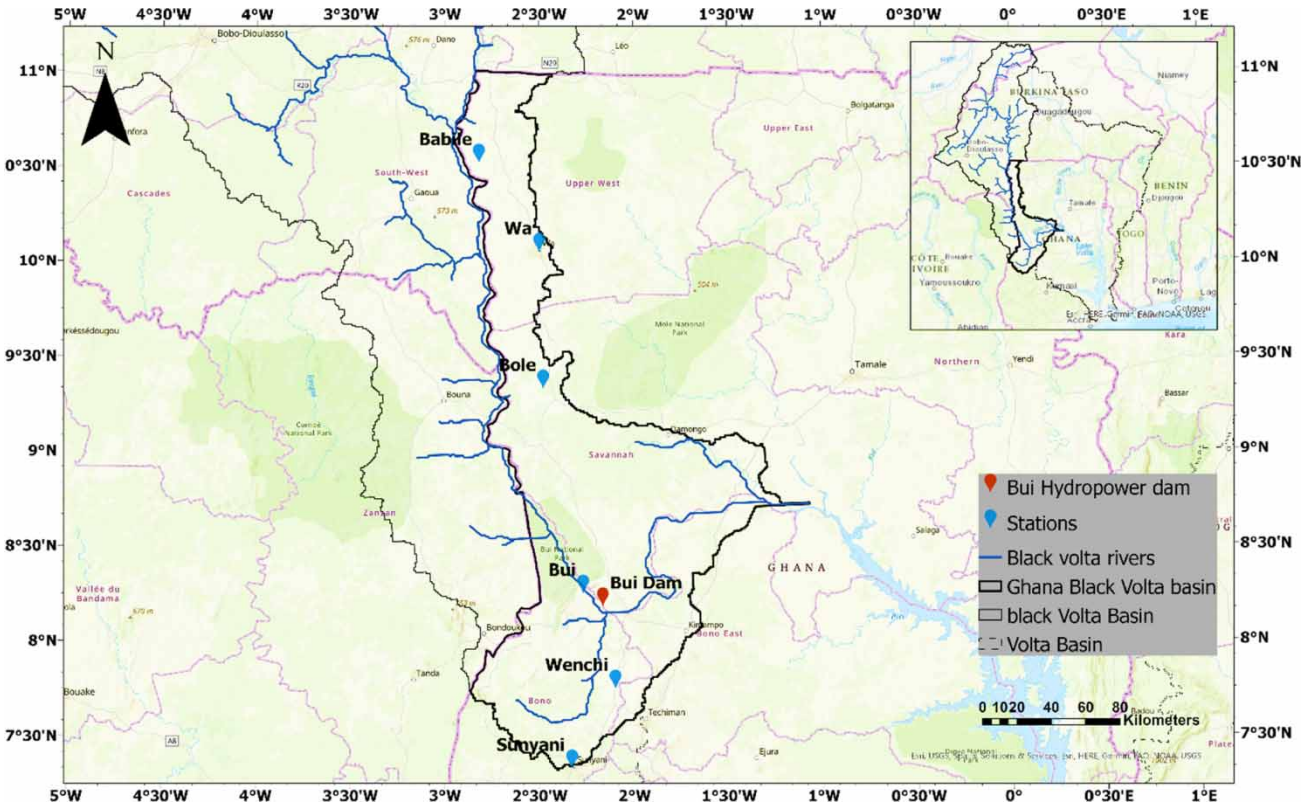

Figure 1 | The BVB of Ghana (author's own construct).

and Mali, respectively (Annor 2012). From Burkina Faso to the Volta Lake, the BVB covers around 1,350 km^2, with major tributaries and a surrounding catchment flowing into the BV river (Smit & Wandel 2006). The villages closest to the basin use the banks of the BVB region mostly for agricultural activities. Bush fallow, which is widely used, is the major type of farming that is being practiced in the basin. Lands are severely deteriorated in terms of soil fertility and physical condition in Ghana's northern BVB, particularly in districts like Lawra, making it impossible to support substantial agricultural production (Greene 2003). The Wa Municipal is a low-lying area with a land area of around 579.86 km^2. The mean annual precipitation varies between 840 and 1,400 mm. In May, the peak monthly maximum temperatures can reach 40 °C. However, temperatures fall as low as 21 °C in December/January (GSS 2021). Crop production is largely due to the district's single maximum rainfall season from May to September/October. Therefore, the basin is an important component of the livelihood of rural folks since it serves the water, food, and energy needs of the people.

2.2. Data used

The ground station Prcp, T_{min}, and T_{max} data were obtained from the Ghana Meteorological Agency (GMet). The dataset used for all the selected stations spans from 1976 to 2016. These stations are located in the BVB (Figure 1). The dataset used was greatly influenced by the availability and consistency of the data collected. This, therefore, influenced the selection of the stations used in the study. For the GCM output, the study used 26 predictors (see Table 1) from the National Centers for

Table 1 | List of predictor variables used for the study

	HadCM3		CanESM2	
No.	Long-name	Short-name	Long-name	Short-name
1	Mean sea level pressure	Mslpaf	Mean sea level pressure	mslp
2	Surface airflow strength	p_faf	Surface airflow strength	p1_f
3	Surface zonal velocity	p_uaf	Surface zonal velocity	p1_u
4	Surface meridional velocity	p_vaf	Surface meridional velocity	p1_v
5	Surface vorticity	p_zaf	Surface vorticity	p1_z
6	Surface wind direction	p_thaf	Surface wind direction	p1th
7	Surface divergence	p_zhaf	Surface divergence	p1zh
8	500-hPa airflow strength	p5_faf	500-hPa airflow strength	p5_f
9	500-hPa velocity	p5_uaf	500-hPa zonal velocity	p5_u
10	500-hPa meridional velocity	p5_vaf	500-hPa-hPa meridional velocity	p5_v
11	500-hPa vorticity	p5_zaf	500-hPa vorticity	p5_z
12	500-hPa geopotential height	p500af	500-hPa geopotential height	p500
13	Mean sea level pressure	p5thaf	500-hPa wind direction	p5th
14	500-hPa divergence	p5_zhaf	500-hPa divergence	p5zh
15	850-hPa airflow strength	p8_faf	850-hPa airflow strength	p8_f
16	850-hPa zonal velocity	p8_uaf	850-hPa zonal velocity	p8_u
17	850-hPa meridional velocity	p8_vaf	850-hPa meridional velocity	p8_v
18	850-hPa vorticity	p8_zaf	850-hPa vorticity	p8_z
19	850-hPa geopotential height	p850af	850-hPa geopotential height	p850
20	850-hPa wind direction	p8thaf	850-hPa wind direction	p8th
21	850-hPa divergence	p8zhaf	850-hPa divergence	p8zh
22	Relative humidity at 500-hPa	r500af	precipitation	Prcp
23	Relative humidity at 850-hPa	r850af	Specific humidity at 500	hPa
24	Near surface relative humidity	rhumaf	Specific humidity at 850	hPa
25	850-hPa geopotential height	shumaf	Surface specific humidity	shum
26	Mean temperature	tempaf	Mean temperature at 2m	temp

Environmental Prediction (NCEP) and the National Center for Atmospheric Research (NCAR) reanalysis data of the Canadian Earth System Model version 2 (CanESM2) as well as the NCEP reanalysis data of the Hadley center Coupled Model version 3 (HadCM3). These reanalysis datasets span from 1961 to 2005 and 1961 to 2001 for NCEP-CanESM2 and NCEP-HadCM3, respectively, and were used for calibration and validation of the models. However, the CanESM2 and HadCM3 GCM data belong to 1961–2100 and 1961–2099, respectively. The CanESM2 and HadCM3 have a spatial resolution of about 2.81 and 2.5°, respectively, with uniform longitude and latitude. The CanESM2 and HadCM3 were used for the future projections downscaling from 2006 to 2100 and 2002 to 2099, respectively. The predictors from the CanESM2 were derived under the RCP 2.6, 4.5, and 8.5 scenarios whereas predictors from the HadCM3 were derived under the A2 and B2 scenarios. The six stations used for the study were located in a single GCM grid box (Box_90X_29Y and Box_128X_36Y for CanESM2 and HadCM3, respectively) for both models.

2.3. Conceptual framework

Figure 2 shows the methodological roadmap for the study. First, predictand variables (Prcp, T_{min}, and T_{max}) are selected as input data. The NCEP reanalysis dataset and GCM outputs provided the set of predictors (see Table 1) from the CanESM2 and HadCM3 that were used for the study. The SDSM is a stochastic and hybrid downscaling simulator created by Wilby and Dawson (2007). The study employed the SDSM in the downscaling process. Unexpected errors such as wrongly encoded and missing data were inspected using the SDSM quality control function, whereas the transform function was used to transform data in a situation where the datasets are not evenly distributed. The preliminary step after attaining the complete datasets is to identify the set of most influencing predictors for each predictand at the station. The fundamental goal of any statistical procedure of downscaling is to empirically establish statistical correlations between predictands and large-scale predictors (Wilby & Dawson 2007). The study of Wilby & Dawson (2007) revealed the potential of selected predictors in defining thickness, atmospheric circulation, moist content, and stability. The selected potential predictor must be simulated well by GCMs and be retrievable from various GCMs sources, as noted by Wilby & Dawson (2007). Most SDSMs can attain a high proportion of success when appropriate predictors are selected (Phuong *et al.* 2020). In this study, the selection of potential predictors was based on correlation, partial correlation, and stepwise regression analysis (Wilby & Dawson 2007). These analyses were conducted to avoid the issue of collinearity and select predictors that have a high and consistent correlation with the local predictands. Therefore, the model is calibrated based on user-specific predictand together with a set of predictor variables. Finally, given atmospheric predictor variables supplied by a climate model (either for present or future climate experiments), the scenario generator was used to produce ensembles of synthetic daily weather series. The documentation of these methods is available elsewhere (Yang *et al.* 2017).

The next stage is the reproduction of daily ensembles for the current period using a well-calibrated model. These models are afterward subjected to the evaluation of their performance using the Taylor diagram and several dimensionless and dimensioned statistics as well as goodness-of-fit. Future climate is subsequently projected based on the selected predictors obtained from the GCM outputs. Finally, the Innovative-Sen trend plots were used to analyze the trend patterns to identify the partial and overall trends in the future climate. However, the delta statistics (Wilby & Dawson 2007) were used to assess the magnitude of changes found between future and baseline periods. It is worth noting that the model calibration and scenario generator SDSM functions were used to calibrate and generate future scenarios, respectively.

2.4. Model performance evaluation

For the evaluation of model performance, the Taylor diagram (Taylor 2001) was used to compare the ensemble mean with individual ensemble members during calibration and validation. The Taylor diagram was used because of its ability to graphically measure the standard deviations, root-mean-square difference, and correlation coefficient of the models and observed data.

The study further employed the Mean Absolute Error (MAE) (Equation (1)), Mean Bias Error (MBE) (Equation (3)), and Coefficient of determination (R^2) (Equation (2)) to evaluate the model performance. For the dimensioned statistics, MAE and MBE were used, whereas the refined index of agreement (with/without baseline adjustments) served as the dimensionless statistics for the study. The values of d_a (Equation (4)) are limited by -1 and $+1$. A good model is signified by a positive value. The study of Legates & Mccabe (2013) further revealed that the model performance is better than the baseline value when d_a is greater than 0.5. The adjustment of baseline values has also been recommended by several researchers (Legates & McCabe 1999; Willmott *et al.* 2009) when assessing the performance of the model for variables of interest,

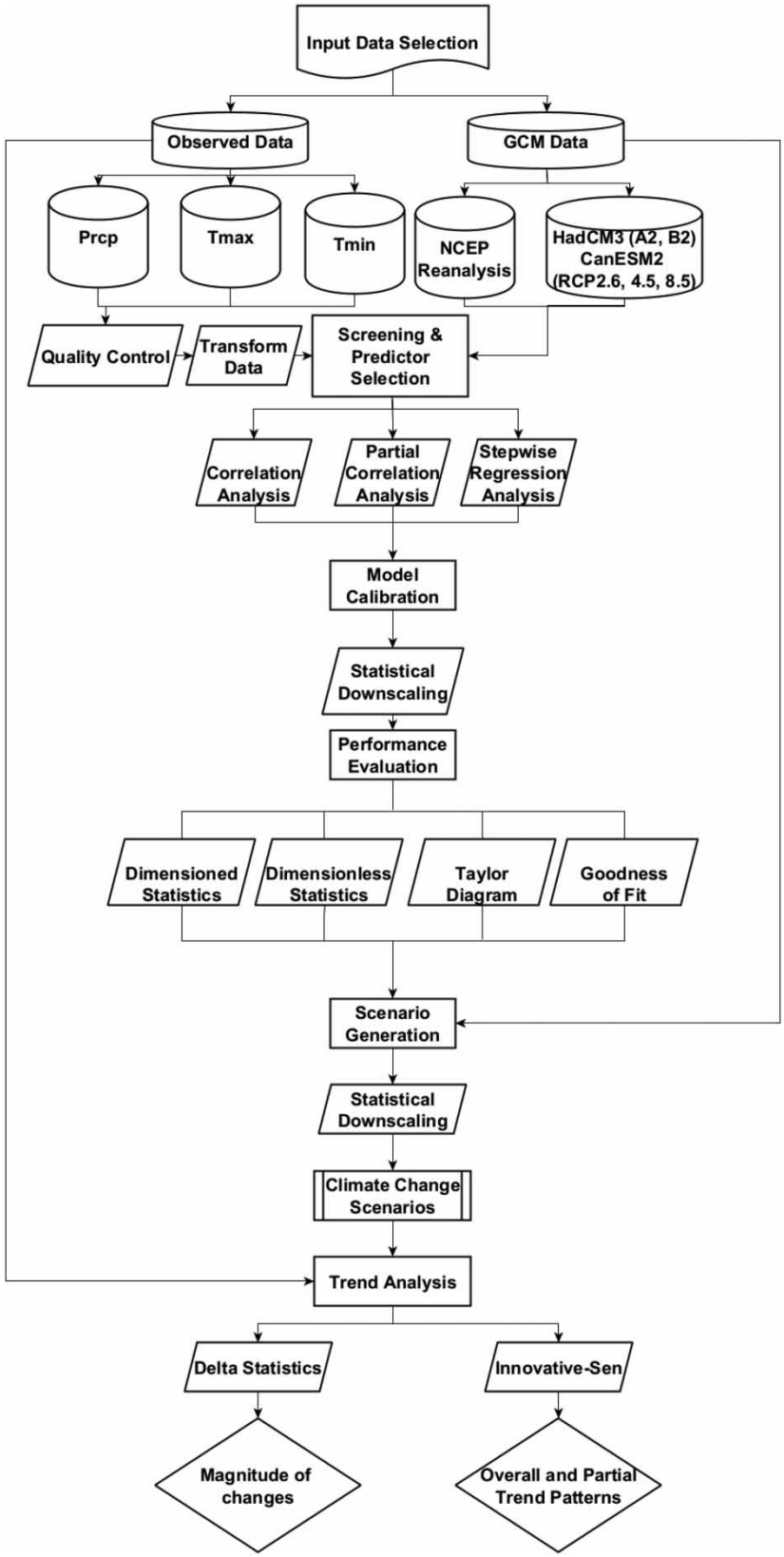

Figure 2 | Methodological roadmap for the study modified from Phuong *et al.* (2020).

which show high seasonal discrepancies. In this index, monthly averages are used as well as the daily values when estimating the refined index of agreement. However, the *MSE*, *RMSE*, and R^2 were used as indicators of goodness-of-fit:

$$MAE = \frac{1}{n}\sum_{i=1}^{n}|y_i - x_i| \tag{1}$$

$$MBE = \frac{1}{n}\sum_{i=1}^{n}(y_i - x_i) \tag{2}$$

$$R^2 = 1 - \sum\frac{(y_o - y_e)^2}{(y_o - y_e)^2} \tag{3}$$

$$d_a = \begin{cases} 1 - \dfrac{\sum_{i=1}^{n}|y_i - x_i|}{c\sum_{i=1}^{n}|x_i - \bar{x}|}, & \text{when } \sum_{i=1}^{n}|y_i - x_i| \le c\sum_{i=1}^{n}|x_i - \bar{x}| \\ \dfrac{c\sum_{i=1}^{n}|x_i - \bar{x}|}{\sum_{i=1}^{n}|y_i - x_i|} - 1, & \text{when } \sum_{i=1}^{n}|y_i - x_i| > c\sum_{i=1}^{n}|x_i - \bar{x}| \end{cases} \tag{4}$$

where n is the length of data; y_i is the predicted value of Prcp, T_{min}, and T_{max}; x_i is the observed value of Prcp, T_{min}, and T_{max}.

The overbars show the means of the daily values for the whole analyzed period. The scaling coefficient c should preferably be set to 2 (Legates & Mccabe 2013; Willmott *et al.* 2015). In estimating the index of agreement with baseline adjustment (d_a'), the mean of the daily values ($\bar{y}$) is replaced by the mean of monthly values ($\overline{y'}$).

2.5. Innovative-Sen trend analysis

The ITA was originally developed by Şen (2012). This method is used to define the partial and overall patterns in a specified hydro-climatic dataset. Compared to other conventional trend analyses such as nonparametric and parametric statistical trend analysis, the ITA process has the comparative advantage of not enabling any restraining assumptions including length of data, serial independence, and normal distribution. The study analyzed the possibilities of multi-duration patterns in the monthly global temperature (Mohorji *et al.* 2017). Thus, the ITA technique was used to assess the patterns of Prcp, T_{min}, and T_{max} between the baseline (1976–2005) and the future (2010–2039, 2040–2069, and 2070–2099) periods based on different scenarios. To plot ITA results, the baseline and future periods are sorted in ascending order and then plotted on the x-axis against the y-axis, respectively. Afterward, a 1:1 (45°) straight line that divides the plot into two equal sections and $\pm 10\%$ error lines is constructed on a Cartesian coordinate system (Figure 3). The upper and lower triangular regions indicate increasing and decreasing trends, respectively, whereas the 45° straight line denotes a trend-free situation. Moreover, evidence shows that trend slop is high when the scatter plot points move far away from the 45° straight line.

3. RESULTS AND DISCUSSION

3.1. Calibration and validation of models

The calibration of both models (CanESM2and HadCM3) was done using 29-year (1976–2005) and 25-year (1976–2001) baseline data, respectively, while validation was done using a 10- (2006–2016) and 14-year (2002–2016) baseline data, respectively. The Taylor diagrams presented in Figure 4 compared the individual ensemble with the corresponding ensemble mean for T_{max}, T_{min}, and Prcp at each station during validation. A closer look at the diagram (Figure 4) reveals that the SDSM provided similar trends across the selected stations for individual predictand variables considering specific locations of all the points on the Taylor diagram. On the disparities of the downscaled results, individual ensembles showed a lower error and higher correlation than the ensemble means across all the stations for T_{max}, T_{min}, and Prcp. However, the ensemble mean of

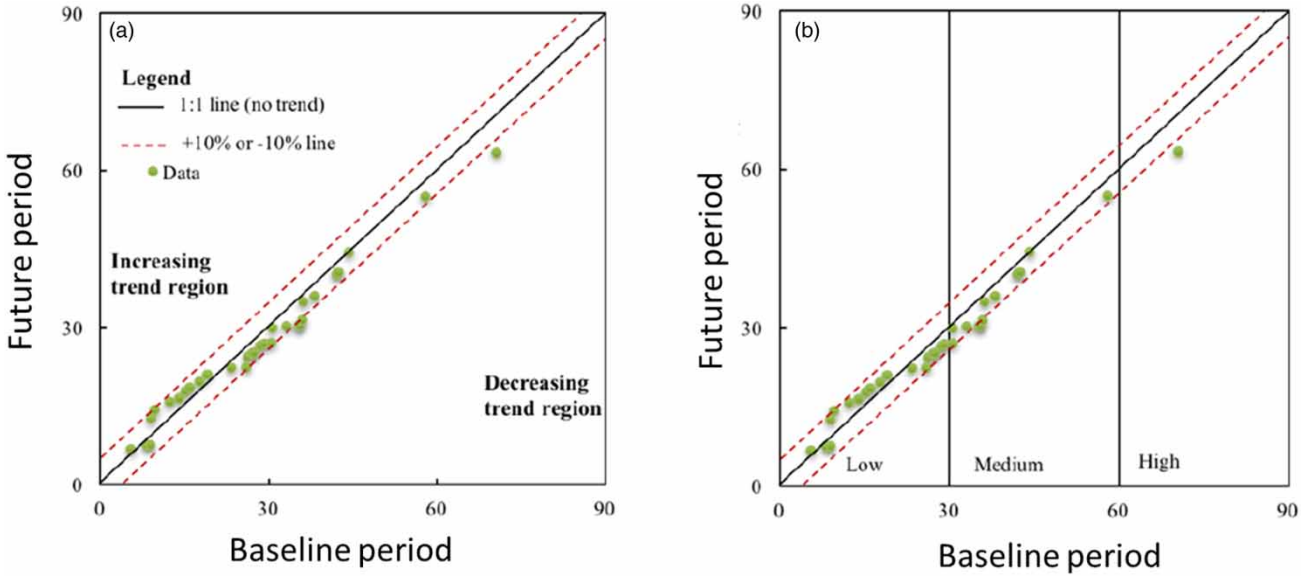

Figure 3 | Illustration of the ITA technique by Şen (2012). (a) Non-monotonic trends and (b) trends of each segment (low, medium, and high). *Source:* Alifujiang *et al.* (2020).

T_{max} at Bui captured the observed standard deviations better than the individual ensembles as the solid points almost fell on the black arc (see Figure 4), indicating the amplitude of disparities of the downscaled output for T_{max} at Bui is similar to the observed. Comparing the downscaled output for the three climatic variables, it is also obvious that the output of Prcp (see Figure 4) reveals a high degree of disparity compared to T_{max} (Figure 4) and T_{min} (Figure 4). This could be attributed to the conditional procedure during the calibration of Prcp. These findings confirm the findings of previous studies (Gulacha & Mulungu 2016; Tarek *et al.* 2016) which found difficulties in downscaling Prcp using the SDSM. Gulacha & Mulungu (2016) further noted that the SDSM may not be the best tool for downscaling Prcp. However, this study's calibration results were higher (see Table 2) compared to previous studies in Africa (Gulacha & Mulungu 2016; Tarek *et al.* 2016; Gebrechorkos *et al.* 2019b). Moreover, the values of the ensemble means were used for further estimations.

On model performance evaluation, using graphical techniques only is not highly recommended. Therefore, in addition to graphical methods, both dimensionless and dimensioned measures are highly recommended (Legates & McCabe 1999; Willmott *et al.* 2015). Table 2 presents dimensioned statistics during calibration and validation results for both models.

For the dimensioned statistics, the values of MAE during calibration ranged from about 0.342–0.574 mm, 0.007–0.093 °C, and 0.011–0.285 °C for Prcp, T_{max}, and T_{min}, respectively (Table 2). It is therefore obvious that the errors of the model during calibration for T_{min} are slightly higher than T_{max}. To compare the two models (HadCM3 and CanESM2), both simulated daily Prcp with similar errors during calibration. However, CanESM2 generally recorded higher errors in predicting daily Prcp during calibration. During validation, the values of MAE ranged from 0.351–1.060 mm, 0.089–0.889 °C, and 0.069–0.295 °C for Prcp, T_{max}, and T_{min}, respectively. This reveals slightly higher model errors during validation for both models especially in simulating T_{max}. However, this is consistent with the findings of Phuong *et al.* (2020). There were fairly similar model errors for both models (HadCM3 and CanESM2) in simulating the daily Prcp and T_{max} during validation. However, CanESM2 recorded more significant model errors than HadCM3 in simulating daily T_{min} during validation. The values of MBE ranging from −0.342 to −0.574 mm, −0.059 to −0.001 °C, and −0.128 to −0.0001 °C for Prcp, T_{max}, and T_{min} respectively show a slight underestimation of predictands during calibration. To compare both models, CanESM2 was found to significantly underestimate daily Prcp and T_{max} compared to HadCM3 (Table 2) during calibration. MBE values ranged from −0.627 to −0.042 mm, −0.049 to 0.187 °C, and −0.274 to −0.043 °C for Prcp, T_{max}, and T_{min}, respectively. Similarly, CanESM2 underestimated daily Prcp, T_{max}, and T_{min} compared to HadCM3 during validation (see Table 2). However, the dimensioned statistical results on validation were generally satisfactory since they fell within an acceptable range on the daily time scale.

Moreover, the goodness-of-fit results from R^2 revealed better performance during calibration and validation. For instance, the values for R^2 ranged from 0.997–0.999, 0.950–0.999, and 0.9713–0.996 for T_{max}, T_{min}, and Prcp, respectively, during

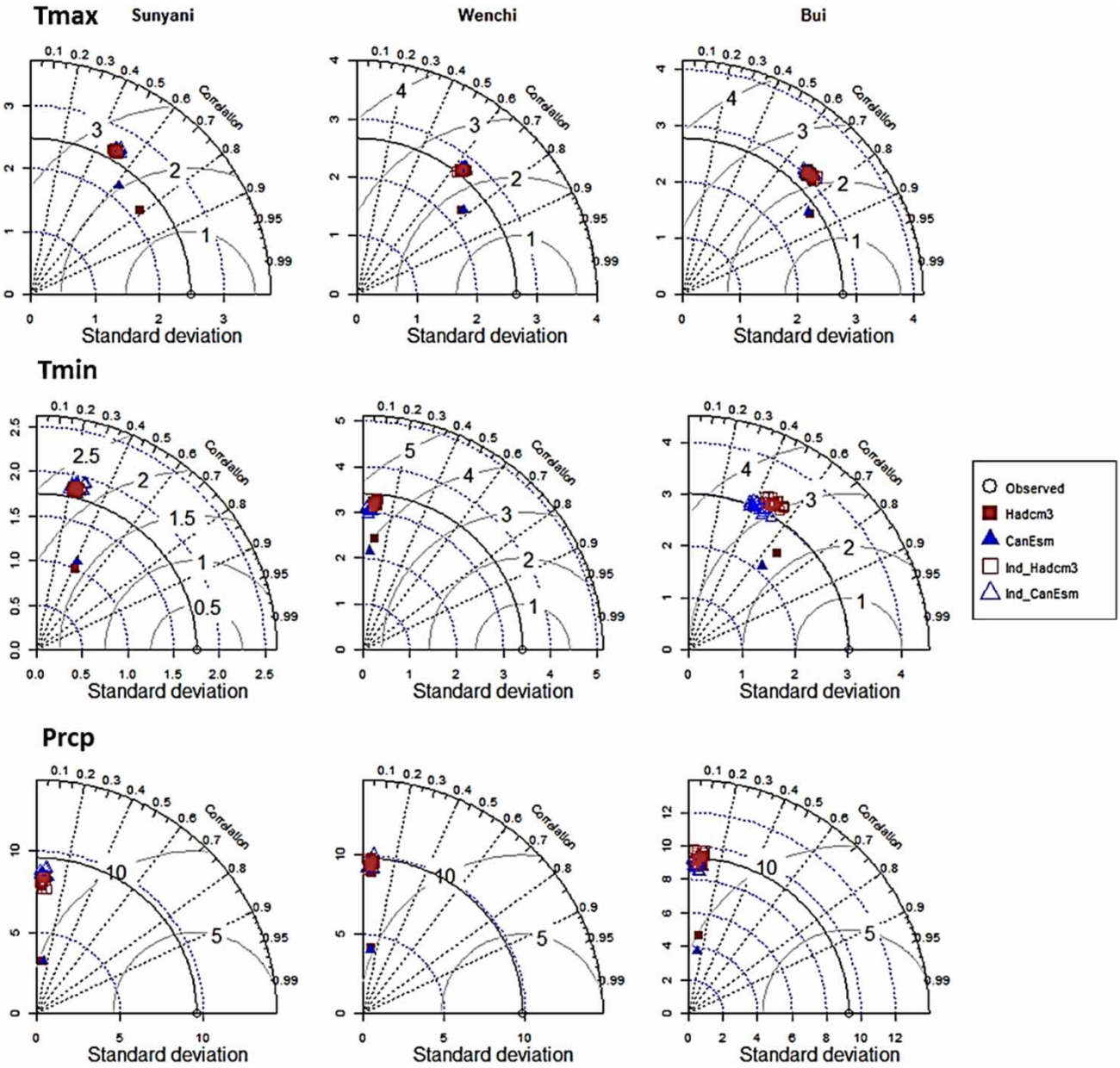

Figure 4 | Taylor diagram comparing an individual ensemble member with a corresponding ensemble mean for T_{max}, T_{min}, and Prcp at some stations during validation.

calibration. Surprisingly, the R^2 values for precipitation were higher during calibration (i.e. between 0.971–0.996). Similarly, other studies (Gebrechorkos *et al.* 2019b) revealed higher performance of the SDSM based on R between 0.79–0.98 in basins of East Africa. The performance improvement observed in this study may be attributed to the long period of calibration (ranging from 25–29 years), which is noted to impact the model's performance. The longer period of calibration is found to generate probability distribution functions in the process of statistical downscaling (Kim *et al.* 2000). However, the values for R^2 dropped during validation as they ranged from 0.802–0.999, 0.955–0.997, and 0.646–0.957 for T_{max}, T_{min}, and Prcp, respectively. The performance of HadCM3 in simulating the daily Prcp during validation was higher than CanESM2 (see Table 2). However, the performance of both models was similar in simulating daily T_{max} and T_{min} during validation. Although the determinants of the goodness-of-fit dropped generally during validation, the performance of both models was better compared to previous studies (Gulacha & Mulungu 2016; Tarek *et al.* 2016) in Africa. Furthermore, the length of data for

Table 2 | Model performance during calibration and validation

Criteria	HadCM3		CanEsm	
T_{max}	Calibration	Validation	Calibration	Validation
Babile				
MAE (°C)	0.018	0.164	0.039	0.134
MBE (°C)	0.002	−0.139	−0.032	−0.065
R^2	0.999	0.998	0.999	0.996
Wa				
MAE (°C)	0.010	0.888	0.063	0.141
MBE (°C)	−0.011	0.180	−0.061	−0.108
R^2	0.999	0.802	0.999	0.998
Bole				
MAE (°C)	0.008	0.161	0.048	0.092
MBE (°C)	−0.001	−0.154	−0.022	−0.078
R^2	0.999	0.998	0.999	0.999
Bui				
MAE (°C)	0.059	0.098	0.093	0.111
MBE (°C)	0.015	−0.049	0.037	0.001
R^2	0.999	0.997	0.999	0.997
Wenchi				
MAE (°C°C)	0.085	0.114	0.081	0.089
MBE (°C)	0.078	−0.104	0.065	−0.067
R^2	0.999	0.998	0.999	0.999
Sunyani				
MAE (°C)	0.007	0.136	0.048	0.196
MBE (°C)	0.003	−0.134	−0.042	−0.187
R^2	0.999	0.998	0.999	0.997
T_{min}				
Babile				
MAE (°C)	0.018	0.129	0.053	0.129
MBE (°C)	0.011	0.011	−0.039	0.011
R^2	0.999	0.997	0.999	0.997
Wa				
MAE (°C)	0.121	0.141	0.084	0.207
MBE (°C)	−0.0001	−0.137	−0.082	−0.207
R^2	0.999	0.993	0.998	0.997
Bole				
MAE (°C)	0.014	0.148	0.014	0.289
MBE (°C)	0.002	−0.108	−0.008	−0.274
R^2	0.999	0.996	0.999	0.989
Bui				
MAE (°C)	0.098	0.137	0.285	0.295
MBE (°C)	0.058	−0.043	0.041	−0.239
R^2	0.996	0.992	0.950	0.955

(*Continued.*)

Table 2 | Continued

Criteria	HadCM3		CanEsm	
T_{max}	Calibration	Validation	Calibration	Validation
Wenchi				
MAE (°C)	0.065	0.069	0.145	0.135
MBE (°C)	−0.056	0.027	−0.128	−0.124
R^2	0.994	0.993	0.953	0.981
Sunyani				
MAE (°C)	0.011	0.108	0.036	0.084
MBE (°C)	−0.004	−0.065	−0.016	−0.056
R^2	0.999	0.971	0.998	0.988
Prcp				
Babile				
MAE (mm)	0.342	0.634	0.431	0.508
MBE (mm)	−0.342	−0.337	−0.431	−0.308
R^2	0.9988	0.952	0.998	0.936
Wa				
MAE (mm)	0.416	0.351	0.453	0.635
MBE (mm)	−0.248	−0.042	−0.240	−0.076
R^2	0.971	0.951	0.9731	0.909
Bole				
MAE (mm)	0.429	0.784	0.408	0.529
MBE (mm)	−0.429	0.169	−0.408	−0.273
R^2	0.996	0.819	0.996	0.875
Bui				
MAE (mm)	0.522	0.946	0.417	1.060
MBE (mm)	−0.522	−0.627	−0.417	−0.288
R^2	0.987	0.881	0.982	0.646
Wenchi				
MAE (mm)	0.486	0.572	0.457	0.766
MBE (mm)	−0.419	−0.500	−0.357	−0.544
R^2	0.976	0.891	0.973	0.851
Sunyani				
MAE (mm)	0.497	0.568	0.574	0.417
MBE (mm)	−0.497	0.254	−0.574	−0.371
R^2	0.994	0.827	0.993	0.957

calibration may have some bearing on the performance of the model. This helps the SDSM to generate probability distribution functions in the process of downscaling (Kim *et al.* 2000). The performance of both models revealed by the goodness-of-fit results during calibration was very high and therefore increased the confidence level of the future projections.

Finally, the study considered only the validation results for a dimensionless statistic (see Figure 5). The refined index of agreement with baseline adjustment (d_a') and without baseline adjustment (d_a) were used. Figure 5 reveals the ability of the SDSM in downscaling daily $T_{\max}$ and $T_{\min}$ as the d_a values ranged from 0.57 to 73 compared to the d_a' values of daily Prcp which ranged from 0.48 to 0.55. The value obtained in this study is slightly lower than the values found in (Najafi & Hessami Kermani 2017; Phuong *et al.* 2020) for Prcp, $T_{\max}$, and $T_{\min}$. Conversely, d_a' values for Prcp, $T_{\max}$, and $T_{\min}$

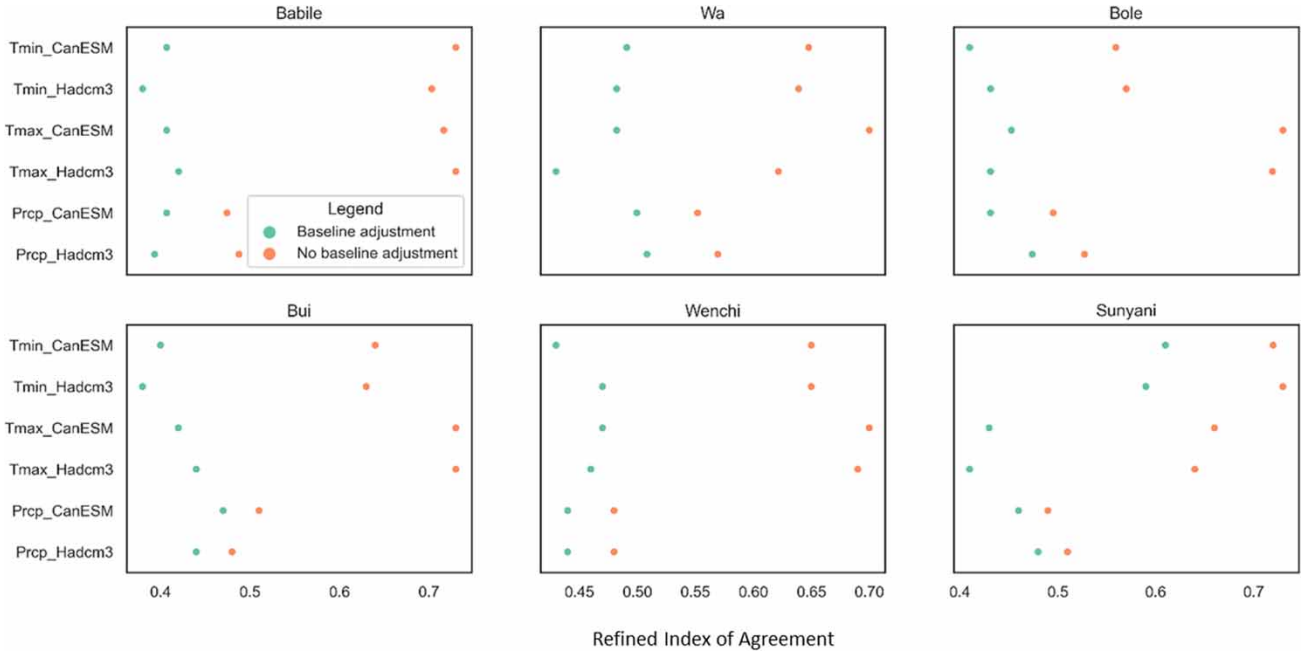

Figure 5 | Validation results for the refined index of agreement with and without baseline adjustment.

ranged approximately from 0.38 to 0.61. These values are lower than their corresponding d_a values. Figure 4 reveals that HadCM3 and CanESM2 have similar ability in predicting T_{max}, T_{min}, and Prcp. Comparing performance, CanESM2 generally performed better than HadCM3 in predicting T_{max} and T_{min} whereas HadCM3 generally performed better than CanESM2 in predicting Prcp. Generally, the values obtained for d_a and d'_a represented by MAE show the extent of mean model error which is lower than the base error during validation represented by two times mean absolute deviation. Therefore, the model that is calibrated can be employed in generating future scenarios.

3.2. Future climate projection

The delta statistics between the baseline period and future periods for Prcp, T_{max}, and T_{min} are presented in Figures 6 and 7. These figures show the expected mean annual Prcp, T_{max}, and T_{min} under the selected scenarios (i.e. A2 and B2 for HadCM3 and RCP 2.6, 4.5, and 8.5) for HadCM3 and CanESM2. Both models generally predict a significant decreasing trend in Prcp taking into consideration near- to far-future periods except in stations such as Babile and Wenchi where CanESM2 projects an increasing trend. Figure 6 presents a detailed description of the future projected changes in annual Prcp. Both models projected near-future to far-future decreases by 2.05–23.89, 5.41–46.35, and 5.84–35.33% in the 2020s, 2050s, and 2080s. For instance, CanESM2 projects increase in Prcp by about 0.89–13.63, 11.61–20.83, and 0.28–27.23% in the three time periods, respectively, at Babile whereas HadCM3 projects decrease by 23.31–23.89, 37.46–46.35, and 11–24.51% in the near, middle, and future periods (i.e. the 2020s, 2050s, and 2080s, respectively). At Wa, both models predicted decreases in the 2050s and 2080s except RCP 8.5 where Prcp is expected to increase by about 82.11% at the end of the 21st century. Prcp is expected to decrease slightly by about 4.78–9.91% in the near to middle future, however, it is expected to decrease significantly by approximately 21.57–28.1% in the far-future as projected by HadCM3 at Bole. CanESM2 however, predicts a drop in Prcp by about 6.79–9.69, 15.74–30.03, and 15.26–35.33% throughout the three time periods, respectively (Figure 6). At Bui, Prcp is projected by CanESM2 and HadCM3 to drop by about 3.96–6.78, 14.77–26.02, and 5.37–18.16% in the 2020s, 2050s, and 2080s, respectively. However, whereas RCP 8.5 predicts a slight increase by about 2.55–13.07% in the near, middle, and far-future periods, RCP 4.5 projects an increase in Prcp in the near-future (about 51.48%), a slight increase in the middle future (about 11.99%) and a significant drop (about 5.37%) in the far-future (see Figure 6). HadCM3 projects a rising trend by about 0.62–0.69, 0.84–8.22, and 11.53–15.66% in Prcp from the near, middle, and far-future, respectively, at Wenchi. However, CanESM2 projects an expected fall by about 2.05–5.45, 5.41–9.24, and 5.84–9.2% in Prcp in the 2020s, 2050s, and 2080s, respectively, except for the spike (of about 5.33%) predicted by RCP 8.5 in the far-future. Both

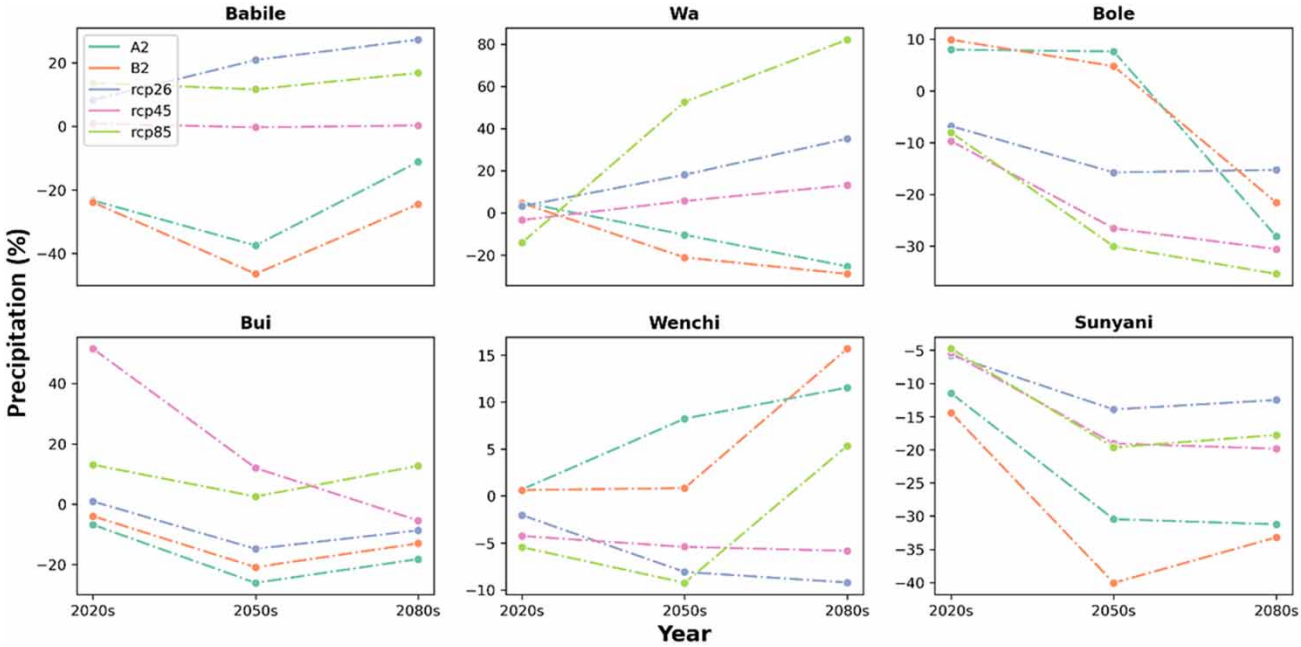

Figure 6 | Forecasted future changes for annual Prcp in the BVB.

models predict an expected decrease (by 5.41–11.49, 13.93–40.04, and 12.51–33.19% for the 2020s, 2050s, and 2080s, respectively) in Prcp throughout the 21st century at Sunyani (see Figure 6). Therefore, there is a general tendency for the occurrence of drought in most parts of the BVB under all the scenarios, especially in the 2080s. The projections by both models are in consonant with the findings of previous studies which indicated decreasing trend of annual Prcp over the BVB (Akpoti *et al.* 2016; Siabi *et al.* 2021). As a result, the water level in the BVB is going to be affected in the future. The BVB hosts the Bui dam which is one of the largest dams in Ghana. The decreasing trend in annual Prcp may contribute to varying reductions in the level of water which is expected to affect hydropower generation by the Bui dam (Akpoti *et al.* 2016; Siabi *et al.* 2021). Agriculture and other related sectors are going to be severely affected since these sectors solely depend on Prcp in the BVB (Kusakari *et al.* 2014). For instance, most agricultural activities such as rice production in northern Ghana are mainly based on irrigation and rainfed agriculture. Therefore, as Prcp drops, rice production is also expected to drop. Therefore, climate change mitigation and adaptation strategies toward drought and floods must be considered with immediate effect by stakeholders and policy-makers in the BVB.

To some magnitude, the findings of this study reveal numerous uncertainties in projecting future daily Prcp. Phuong *et al.* (2020) noted that the projected climate uncertainties are mostly attributed to internal climate variabilities, downscaling tools and methods, and the data used (which includes predictands and predictor variables used). The study employed CanESM2 and HadCM3 predictors which represent manifold emission scenarios. Therefore, other downscaling techniques such as LARS-WG, Bias correction, and Machine Learning approaches can be applied along with the SDSM (Etemadi *et al.* 2014). Phuong *et al.* (2020) also recommended the use of more than one potential predictor set for individual climate data at each station to reach a plausible range of climate variation in future periods.

Moreover, there is an expected high warming tendency in the BVB as T_{max} is projected to record a high magnitude of warming at all the selected stations (Figure 7). Figure 7 reveals that there is an expected minimal variation in T_{max} in the 2020s under all the scenarios. However, the T_{max} is expected to vary significantly in the magnitude of warming in the 2050s and 2080s under all the scenarios. For instance, T_{max} is projected to increase by 0.008–0.52 °C in the 2020s compared to the baseline period. However, T_{max} has a high tendency to generally increase under both models by 0.007–1.39 °C in the 2050s and 0.22–2.44 °C in 2080s compared to the baseline period. However, the highest T_{max} is expected to occur at Wa under the A2 scenario (see Figure 7). Sunyani is projected to be the coldest station compared to the other stations (where the change in T_{max} is $<$0.8 °C). Similarly, T_{min} is generally expected to generally increase by 0.009–0.47, 0.006–0.65, and 0.002–1.83 °C as projected by both models across the periods (Figure 7). Generally, the projections of HadCM3 for T_{max} and T_{min} under

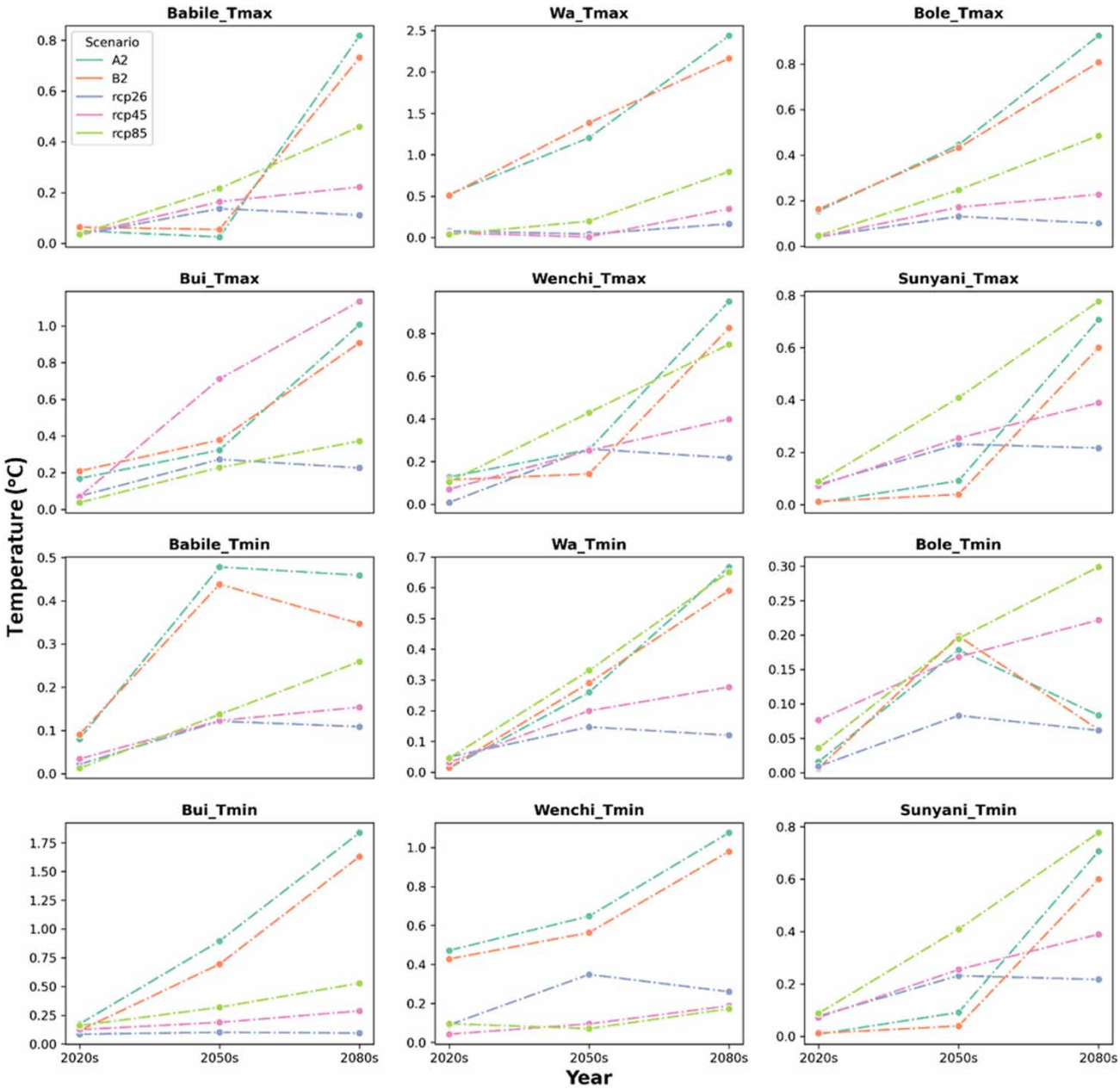

Figure 7 | Forecasted future changes for annual T_{max} and T_{min} in the BVB.

the A2 and B2 scenarios were found to be higher than that of the CanESM. The findings of this study are in line with a previous study that found that temperatures are projected to increase in the BVB (Siabi *et al.* 2021).

Aside from estimating the delta statistics for trend analysis purposes, the study applied the ITA technique to the selected stations. For interpretation of the ITA plot, it is necessary to add the ± 10 error line and divide the plot into three segments that are low, medium, and high. The purpose of these error lines is to ensure a clear understanding of the spacing of the data points from the trendless line without any statistical connotations. Thus, the study also relates to the identification of partial and overall trends between the 2020s, 2050s, and 2080s and the baseline period under different scenarios. The Innovative-Sen trend plots were applied to ascertain whether the annual climate is expected to increase or decrease based on the location of the climate variable falling on the plot.

Figures 8 and 9 present the results from the ITA for Prcp, T_{max}, and T_{min}. The results show that Prcp is expected to generally decrease significantly at stations such as Babile, Wa, and Sunyani (see Figure 8) under most scenarios. For instance, at Babile,

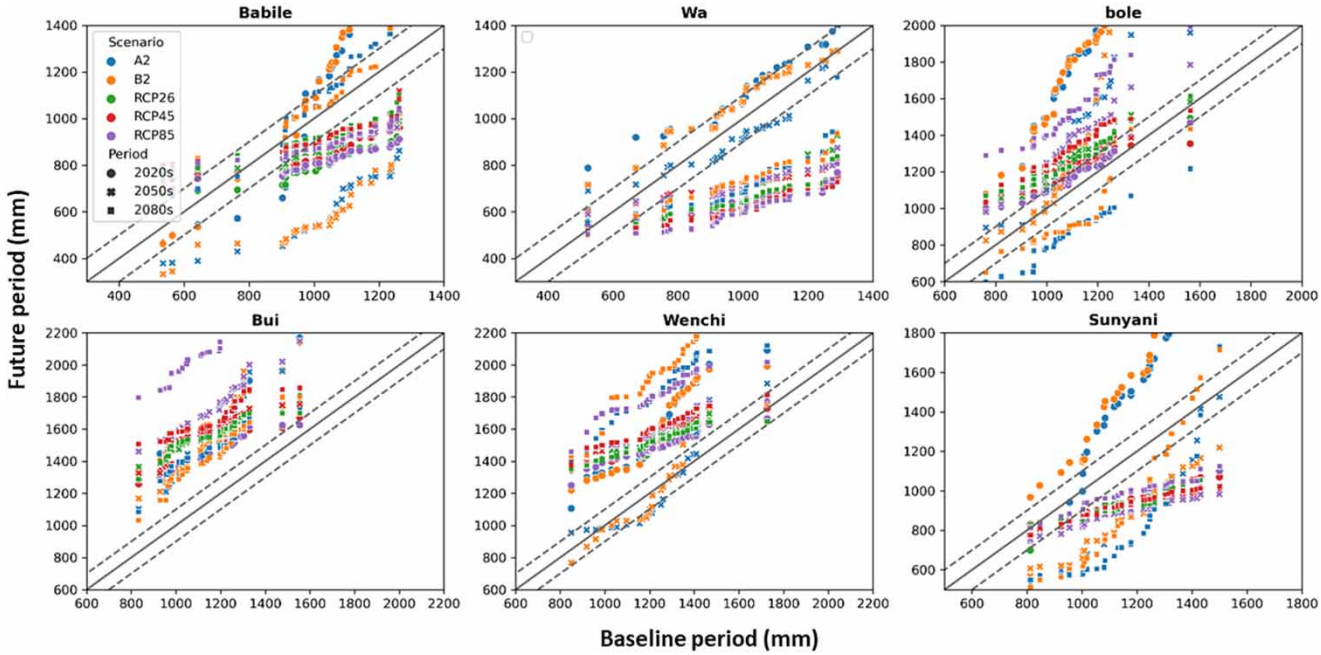

Figure 8 | Near-, middle-, and far-future periods and baseline period comparison of Prcp using an innovative-Sen trend plot under different scenarios for each station. Please refer to the online version of this paper to see this figure in colour: http://dx.doi.org/10.2166/nh.2022.018.

Prcp is expected to decline especially in the 2050s under the A2 and B2 scenarios (see Figure 8). The decline is expected to be severe since the star blue and orange points fell within the medium to high segment of the lower diagonal (Figure 8). Additionally, Prcp under the RCP 2.6, 4.5, and 8.5 is expected to decline severely, especially in the 2020s and 2080s. However, Prcp is expected to increase severally under the A2 and B2 scenarios in the 2020s. An extreme increase in Prcp is expected since the round blue and yellow points scattered in the medium to high segment of the upper diagonal (see Figure 8). The trend of Prcp at Wa is similar to that of Babile. However, Prcp is expected to decline severely in the 2080s, especially under RCPs 4.5 and 8.5. Similar to Babile, Prcp is expected to increase in the 2020s and 2050s under the A2 and B2 scenarios at Wa (Figure 8). This can be seen as the round blue and orange as well as star blue and orange points falling in the medium to high segment above the 45° line (see Figure 8). Just like Babile and Wa, Prcp is expected to decline in the RCP scenarios in the 2020s, 2050s, and 2080s and increase under the A2 and B2 scenarios in the 2020s (Figure 8). Thus, most data points fell below the 1:1 line, implying an overall downward trend at this station. However, the increase and drop are expected to be moderate since most of the data points fell in the low to the medium segment of the plot. For Bole, Bui, and Wenchi, Prcp is expected to generally increase gently under most scenarios in the 2020s, 2050s, and 2080s (see Figure 8). However, A closer look at Figure 8 reveals filled circular and star points in purple and orange, respectively, representing RCP 8.5 and B2 scenarios in the 2020s and 2050s falling alongside the 1:1 (45°) straight line and within the ± 10 error lines indicating an insignificant increase in Prcp at Bole. Generally, most of the data points fell within the low to moderate segment implying a gradual increasing trend in Prcp at Bole, Bui, and Wenchi. This is in line with the findings of Kaboré *et al.* (2015) where Prcp is expected to marginally increase in the Massili basin, Burkina Faso. However, the increase in Prcp projected at Babile is expected to be extreme. Extreme Prcp is known to be the major cause of perennial flooding in northern Ghana, especially in the Upper West region where Babile is located.

The decline in Prcp revealed by the findings of the study agrees with the findings of Yira *et al.* (2016) where Prcp is expected to drop by 9–12%. The findings of Gulacha & Mulungu (2016) also revealed a change in Prcp by −44 to 648% and −37 to 346% under the A2 and B2 scenarios, respectively. Moreover, Asante & Amuakwa-Mensah (2015) revealed that climate change together with detrimental anthropogenic activities concerning land use may worsen desertification in northern Ghana. Population growth which triggers expansion of settlements, agriculture, and over-exploitation of natural resources in an unsustainable manner in a desertification susceptible zone of Ghana may be a cause. However, this is worsened by the decline in Prcp in northern Ghana. This reveals a high probability of desertification.

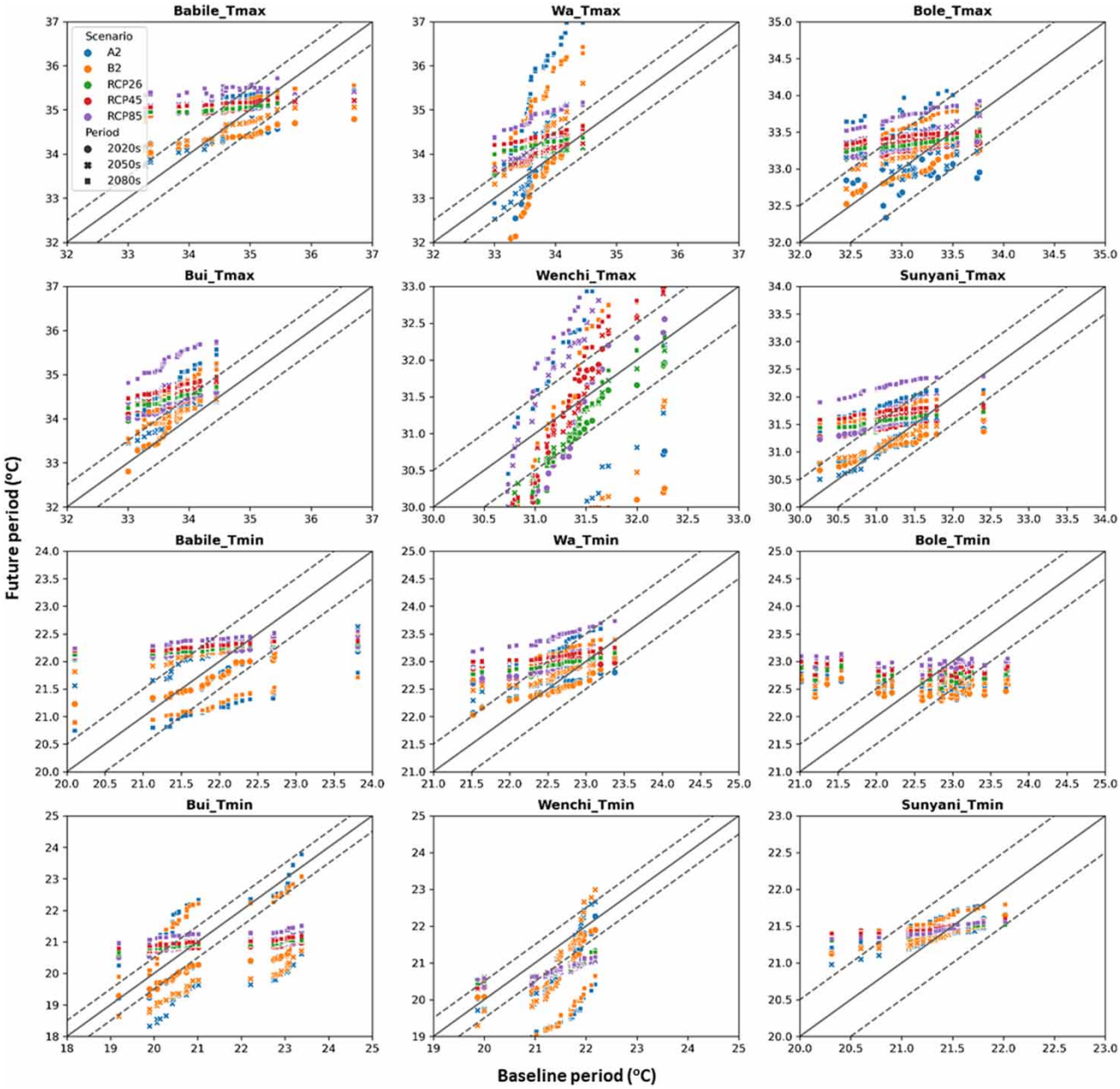

Figure 9 | Near-, middle-, and far-future periods and baseline period comparison of T_{max} and T_{min} using an innovative-Sen trend plot under different scenarios for each station. Please refer to the online version of this paper to see this figure in colour: http://dx.doi.org/10.2166/nh.2022.018.

The mixed trend of the expected Prcp under all the scenarios agrees with the findings of Kebede *et al.* (2013) where Prcp in the Baro-Akobo basin of Ethiopia is expected to change by −2 to 21%. Therefore, Yira *et al.* (2016) noted that the negative and positive Prcp trends reemphasize the discourse on the importance of the trend rather than the magnitude of change in projected Prcp over West Africa.

Generally, T_{max} exhibits a significant increasing trend under all the scenarios as most of the scatter points fell in the upper triangular area of the plot (Figure 9). For Babile, there is an expected low to medium increasing trend in T_{max} especially in the 2080s under the RCP 8.5. This is denoted by purple square points falling at the upper diagonal. However, this increase is expected to be gradual since the point fell within the lower to medium part of the upper diagonal (see Figure 9). Similarly, stations such as Bui, Wenchi, and Sunyani are expected to observe a low to medium increase in the 2080s especially

under RCP 4.5 and the worst-case scenario (RCP 8.5). Also, Wa and Bole are expected to observe a gradual increase in T_{max} in the 2080s, however, this is expected to occur under the A2 scenario. This is signified by the blue square points scattering in the lower to medium part of the upper diagonal (see Figure 9). The projected increasing trend in T_{max} is in line with the findings of Kaboré *et al.* (2015) and Badou *et al.* (2018). For instance, Kabore found that T_{max} is expected to increase by 1.8 and 3.0 °C under the RCP 4.5 and RCP 8.5, respectively, in the Massili basin of Burkina Faso. Similarly, the study of Oyerindé (2016) revealed that temperature is expected to increase between 5 and 10% under RCP 4.5 and 5 and 20% under RCP 8.5 in the Niger river basin by the end of the 21st century. Moreover, Kebede recorded an increase in temperature under the B1 scenario relative to A1B for 50 and 40% of the stations for T_{max} and T_{min}, respectively.

Although the findings of these studies (Kebede *et al.* 2013; Kaboré *et al.* 2015; Oyerindé 2016; Badou *et al.* 2018) are higher than the current study, this could be largely due to the relatively high temperatures observed in Niger and Burkina Faso compared to Ghana. Conversely, stations such as Wa, Bui, Wenchi, and Sunyani are expected to record a gradual decrease in T_{max} in the 2020s under the B2 scenario. This is signified by orange round points falling in the low to medium segment below the 45° line (Figure 9). However, the decreasing trend in T_{max} is expected to be high at Wa in the 2020s under the B2 scenario (Figure 9). Also, Bole is expected to record a gradual decrease in T_{max} in the 2020s, however, this is expected to occur under the A2 scenario.

T_{min} is projected to generally follow the gradually increasing trend of T_{max} into the future under all the scenarios. For example, T_{min} shows a gradual increase, especially in the 2080s under the RCP 8.5 scenario at Babile, Wa, and Bole (see Figure 9). This is shown by the purple square point scattering in the lower to medium part above the 45° line. Similarly, T_{min} is expected to increase gradually at Bui and Sunyani in the 2080s under the RCP 8.5. For some reason, T_{min} is expected to decrease gradually in all three periods under all scenarios at Wenchi. This is seen as most of the scatter points fell at the lower triangular portion of the plot (see Figure 9). For the assessment of partial-trend, T_{max}, and T_{min} show the same partial-trend patterns. These partial trends are particularly likely to be more tangible when their respective values increase, indicating an obvious occurrence of hot weather events in future periods. However, the decreasing trends in T_{min} at some stations show the discontinuation of warming by the end of the 21st century. This is in line with the findings of the IPCC (2014). This validates the findings of Kebede *et al.* (2013) after downscaling T_{min} and T_{max} under the A1B scenario. T_{min} was found to decrease in the future (Kebede *et al.* 2013), however, the decrease in T_{min} is expected to be drastic compared to the current study.

4. IMPLICATIONS OF THE PROJECTED CLIMATE CHANGES IN THE BVB

In the face of higher temperatures, an outbreak of diseases is expected to increase. Previous studies have revealed the outbreak of diseases such as measles, cholera, diarrhea, guinea worm, and cerebrospinal meningitis among others as a result of the increase in temperature and decrease in Prcp in Ghana (Asante & Amuakwa-Mensah 2015). Again, an increase in temperatures coupled with poor drainage systems may increase vector-borne diseases such as malaria Haines *et al.* (2006) found that climate change may affect the spread of mortality and morbidity through physical impacts of exposure to high and low temperatures.

Moreover, crop yield in the basin is expected to be affected due to drought. Kusakari *et al.* (2014) found that the Upper West region located in the northern part of the BVB of Ghana is vulnerable to climate variability and extreme conditions such as floods and droughts severe temperatures. This affects agriculture which serves as the major livelihood (GSS 2021), and renders it defenseless in the face of harsh climate conditions. Studies (Dayour *et al.* 2014; Gordon *et al.* 2019) revealed that most agricultural activities in the north of Ghana rely tangibly on the rainfed system, making them susceptible to climate-related extremes. For instance, rice is a major crop produced in northern Ghana that runs on irrigation schemes and the rainfed uplands and lowlands system. Therefore, under extreme conditions, rice production is likely to drop. Knox *et al.* (2011) found that there is a projected variation of about −8% in rice production. Again, wheat production is expected to drop by about 99% over West Africa in the 2080s. However, maize production is expected to drop by 1–7%. Also, Boatemaa *et al.* (2022) revealed that crop irrigation requirements for tomatoes at Bole are expected to increase by 21 and 27% under RCPs 4.5 and 8.5, respectively, in the 2080s. Perennial water scarcity is known to be predominant in the Savannah zone where the BVB lies. This poses a threat to dry-season farming, mostly rainfed in the basin. For this reason, there is an expected increase in food prices and seasonal migration of households to southern Ghana in the dry season in quest of fertile lands and mining sites to feed family members in the future.

Moreover, Bessah *et al.* (2022) showed that the stations in the transitional zone (Wenchi and Sunyani) aligned to one of the three major climatic zones characterized by similar factors while delineating the climatic zones in Ghana. Therefore, a future shift in temperatures, rainfall seasonality, or monthly patterns may trigger a potential reclassification of the agroecological zones in the BVB. This will help in formulating adequate policies to manage climate-related interventions such as planting for food and jobs. Future water requirements for the production of food and energy as well as domestic sustenance are expected to surge by 34% by 2030 (Opoku *et al.* 2022).

Flooding events are expected to occur in the face of increased precipitation events. This calls for mitigation and adaptation strategies for floods, especially in the 2050s and 2080s. The report of OCHA (2007a) recorded the negative impacts of a catastrophic flood that hit West Africa in 2007. This led to the loss of lives, severe food shortage, and polluted water bodies in the BVB. About 56 people lost their lives and 332,600 people were affected in the northern, Upper West, and East region of Ghana (OCHA 2007b). Sawai *et al.* (2014) noted that, despite the BVB being located downstream in the semi-arid zone, floods and droughts are the main challenges. For instance, another devastating flood that occurred in August 2021 after a 12-hour downpour in the Upper West region left some 1,605 people in the Jirapa district, Lawra municipality, and the Nadowli-Kaleo district greatly affected (Mordey 2021). About 722 farms were lost as a result. Again, approximately 336 people were displaced and 155 houses were destroyed. Also, farmlands, communities, and irrigation sites were flooded along the Nadowli-Tangasie highway. The main bridge on the Wa-Hale Road that links the Jirapa, Nandom municipalities, Nadow-Kaleo districts to Wa was washed away. This calls for an urgent climate adaptation and mitigation actions to abate the adverse effects of climate change to make cities in the BVB safer, sustainable, inclusive and resilient which addresses the sustainable development goals 11 and 13.

Finally, in the face of a drop in precipitation events, water levels in the basin are expected to fall, adversely affecting the Bui dam's hydropower operations. In 2014, the dam recorded a drop in water level by about 5 m below the maximum reservoir level of 183 m above sea level at an elevation of about 177.9 m above sea level (Bui Power Authority 2014). Therefore, the Bui Power Authority must plan strategically to meet extreme climate changes so that the dam can operate above the projected minimum of 172.09 m above sea level under varying climates by the end of the 21st century.

5. CONCLUSION

The study successfully employed the SDSM tool to downscale daily Prcp, T_{max}, and T_{min} and generated future climate projections using HadCM3 and CanESM2 GCM predictors over the BVB of Ghana. The performance of the model was evaluated based on Taylor diagrams, dimensionless, dimensioned, and goodness-of-fit statistics. The calibrated models can be utilized for future scenario development because the statistics of the validated models were within the permitted range. The performance of the SDSM was found to be better in downscaling daily T_{max} and T_{min} compared to Prcp as shown by the various statistics used.

The trend analysis of projected future climate changes by delta statistics conforms with the results of the ITA. T_{max} was projected to increase in the BVB at a higher degree compared to T_{min}. T_{max} and Tmin are expected to increase by 0.22–2.44 and 0.002–1.83 °C in 2080s, respectively, which are relatively higher compared to the values of the other scenarios as revealed by the delta statistics and the relative location of the scatter points on the ITA plots. Concerning daily Prcp, there was a higher magnitude of variability in the downscaled outputs compared to T_{max} and T_{min}. The future Prcp projected by HadCM3 and CanESM2 indicated a decreasing trend as revealed by the delta statistics and ITA plots. Both models projected near- to far-future decreases by 2.05–23.89, 5.41–46.35, and 5.84–35.33% in the 2020s, 2050s, and 2080s. In summary, the findings of this study infer that the BVB has a high tendency of becoming drier and hotter in future periods, which may lead to potential challenges relating to water, food, and energy consumption. The findings of the study are therefore expected to inform policies in Ghana, especially related to water, food, and energy in the basin, and are informative for pragmatic climate adaptation and mitigation strategies. This signifies there must be an urgent diversification of energy sources by policymakers and stakeholders to develop a more resilient energy sector to support energy demands especially during severe water drops which leads to variabilities in hydropower generation. Therefore, energy providers as well as the government of Ghana must consider investing in renewable energy sources such as thermal power plants and solar energy to supplement electricity generation. Moreover, energy sector investors must critically consider the effects of rainfall and temperature on potential energy generation. Beyond this, the government and policy-makers must foster the 'Green Ghana' agenda to support the decentralization of the prime goal of climate resilience to the grassroot level. Again, policy-makers and stakeholders must

consider formulating policies that aim at mitigating the negative impacts of floods and droughts such as the utilization of rainwater harvesting systems as a potential for drought and flood mitigation, the design of infrastructure and production schemes to cater for higher risks of damages due to drought or floods, the development and implementation of early warning systems as well as the effective and efficient management of various water and agricultural resource projects in the BVB. Such climate actions improve the interdependency between people and their natural environment. The findings of the study are expected to influence evidence-based decision-making by stakeholders to directly relate climate actions to pressing needs based on scenario modeling. However, the study was limited to CMIP3 and CMIP5, future studies should consider socio-economic parameters that influence climate change in the BVB. Therefore, detailed future analysis is required to explore the new CMIP6 data under the shared socio-economic pathway scenarios.

FUNDING

This research received no funding.

DATA AVAILABILITY STATEMENT

Data cannot be made publicly available; readers should contact the corresponding author for details.

CONFLICT OF INTEREST

The authors declare there is no conflict.

REFERENCES

Akpoti, K., Antwi, E. O. & Kabo-bah, A. T. 2016 Impacts of rainfall variability, land Use and land cover change on stream flow of the Black Volta Basin, West Africa, 1–24. https://doi.org/10.3390/hydrology3030026.

Alifujiang, Y., Abuduwaili, J., Maihemuti, B., Emin, B. & Groll, M. 2020 Innovative trend analysis of prcp in the Lake Issyk-Kul Basin, Kyrgyzstan. *Atmosphere (Basel)* **11** (4), 1–16. 2020, doi: 10.3390/atmos11040332.

Anandhi, A., Frei, A., Pierson, D. C., Schneiderman, E. M., Zion, M. S., Lounsbury, D. & Matonse, A. H. 2011 Examination of change factor methodologies for climate change impact assessment. *Water Resources Research* **47** (3), 1–10. https://doi.org/10.1029/2010WR009104

Annor, F. 2012 Diagnostic study of the Black Volta Basin in Ghana. *Allwaters Consult Limited* **33**, 145.

Asante, F. A. & Amuakwa-Mensah, F. 2015 Climate change and variability in Ghana: stocktaking. *Climate* **3** (1), 78–99. https://doi.org/10.3390/cli3010078

Awotwi, A., Annor, T., Anornu, G. K., Quaye-Ballard, J. A., Agyekum, J., Ampadu, B., Nti, I. K., Gyampo, M. A. & Boakye, E. 2021 Climate change impact on streamflow in a tropical basin of Ghana, West Africa. *Journal of Hydrology: Regional Studies* **34**, 100805. https://doi.org/10.1016/j.ejrh.2021.100805

Badou, D. F., Diekkrüger, B., Kapangaziwiri, E., Mbaye, M. L., Yira, Y., Lawin, E. A., Oyerinde, G. T. & Afouda, A. 2018 Modelling blue and green water availability under climate change in the Beninese Basin of the Niger River Basin, West Africa. *Hydrological Processes* **32** (16), 2526–2542.

Bessah, E., Amponsah, W., Ansah, S. O., Afrifa, A., Yahaya, B., Wemegah, C. S., Tanu, M., Amekudzi, L. K. & Agyare, W. A. 2022 Climatic zoning of Ghana using selected meteorological variables for the period 1976–2018. *Meteorological Applications* **29** (1). https://doi.org/10.1002/met.2049

Boatemaa, A., Incoom, M. & Odai, S. N. 2022 Impacts of climate change on crop and irrigation water requirement in the Savannah regions of Ghana **00** (0), 1–20. https://doi.org/10.2166/wcc.2022.129

Bui Power Authority 2014 *Bui Reservoir Operations – July 2014*.

Campozano, L., Tenelanda, D., Sanchez, E., Samaniego, E. & Feyen, J. 2016 Comparison of statistical downscaling methods for monthly total precipitation: case study for the Paute River Basin in southern Ecuador. *Advances in Meteorology* **2016**. https://doi.org/10.1155/2016/6526341.

Dayour, F., Yendaw, E. & Jasaw, G. 2014 Local residents' perception and adaptation/coping strategies to climate induced disasters in Bankpama, Wa West District, Ghana. *International Journal of Development and Sustainability* **3** (12), 2186–2205.

Dixon, K. W., Lanzante, J. R., Nath, M. J., Hayhoe, K., Stoner, A., Radhakrishnan, A., Balaji, V. & Gaitán, C. F. 2016 Evaluating the stationarity assumption in statistically downscaled climate projections: is past performance an indicator of future results? *Climatic Change* **135** (3–4), 395–408. https://doi.org/10.1007/s10584-016-1598-0.

Dosio, A. & Panitz, H. J. 2016 Climate change projections for CORDEX-Africa with COSMO-CLM regional climate model and differences with the driving global climate models. *Climate Dynamics* **46** (5–6), 1599–1625. https://doi.org/10.1007/s00382-015-2664-4.

Etemadi, H., Samadi, S. & Sharifikia, M. 2014 Uncertainty analysis of statistical downscaling models using general circulation model over an international wetland. *Climate Dynamics* **42** (11–12), 2899–2920. https://doi.org/10.1007/s00382-013-1855-0.

Gebrechorkos, S. H., Bernhofer, C. & Hülsmann, S. 2019a Impacts of projected change in climate on water balance in basins of East Africa. *Science of the Total Environment* **682**, 160–170. https://doi.org/10.1016/j.scitotenv.2019.05.053.

Gebrechorkos, S. H., Hülsmann, S. & Bernhofer, C. 2019b Statistically downscaled climate dataset for East Africa. 2–9. https://doi.org/10.1038/s41597-019-0038-1.

Gordon, Y. Y., Odame, A. D. & Victor, O. 2019 Women Smallholder Farmers' Adaptation to Climate Variability Derivatives in Savannah Ecological Zone, Ghana. In: *Sustainable Development in Africa: Case Studies* (M. Nagao, J. Masinia & A. Alhassan, eds). Spears Media Press, USA, p. 93.

Greene, W. H. 2003 *Econometric Analysis*. Pearson Education India, Upper Saddle River, New Jersey.

GSS 2021 *Ghana 2021 Population and Housing Census*. General report volume 3A. 3A.

Gulacha, M. M. & Mulungu, D. M. M. 2016 Generation of climate change scenarios for precipitation and temperature at local scales using SDSM in Wami-Ruvu River Basin Tanzania. *Physics and Chemistry of the Earth* **100**, 62–72. https://doi.org/10.1016/j.pce.2016.10.003.

Haines, A., Kovats, R. S., Campbell-Lendrum, D. & Corvalan, C. 2006 Climate change and human health: Impacts, vulnerability and public health. *Public Health* **120** (7), 585–596. https://doi.org/10.1016/j.puhe.2006.01.002.

Hassan, Z., Shamsudin, S. & Harun, S. 2013 Application of SDSM and LARS-WG for simulating and downscaling of rainfall and temperature. *Theoretical and Applied Climatology* **116** (1–2), 243–257. https://doi.org/10.1007/s00704-013-0951-8.

IPCC 2007 Summary for Policymakers. In: *Climate Change 2007: The Physical Science Basis. Contribution of Working Group I to the Fourth Assessment Report of the Intergovernmental Panel on Climate Change* (Qin, D., Manning, M., Chen, Z., Marquis, M., Averyt, K., Tignor, M. & Miller, H. L., eds.). Cambridge University Press, New York, Geneva, pp. 996. https://doi.org/10.1038/446727a.

IPCC 2014 Part A: Global and Sectoral Aspects. (Contribution of Working Group II to the Fifth Assessment Report of the Intergovernmental Panel on Climate Change). In: *Climate Change 2014: Impacts, Adaptation, and Vulnerability*, p. 1132. https://www.ipcc.ch/pdf/assessment-report/ar5/wg2/WGIIAR5-FrontMatterA_FINAL.pdf.

Iwadra, M. 2019 Evaluation of future climate using SDSM and secondary data (TRMM and NCEP) for poorly gauged catchments of Uganda : the case of Aswa catchment. *Theoretical and Applied Climatology* **137**, 2029–2048.

Kabo-Bah, A. T., Diji, C. J., Nokoe, K., Mulugetta, Y., Obeng-Ofori, D. & Akpoti, K. 2016 Multiyear rainfall and temperature trends in the Volta River basin and their potential impact on hydropower generation in Ghana. *Climate* **4**, 4. https://doi.org/10.3390/cli4040049.

Kaboré, E., Nikiema, M., Ibrahim, B. & Helmschrot, J. 2015 Merging historical data records with MPI-ESM-LR, CanESM2, AFR MPI and AFR 44 scenarios to assess long-term climate trends for the Massili Basin in central Burkina Faso. *International Journal of Current Engineering and Technology* **5**, 1846–1852.

Kebede, A., Diekkrüger, B. & Moges, S. A. 2013 An assessment of temperature and precipitation change projections using a regional and a global climate model for the Baro-Akobo Basin, Nile Basin, Ethiopia. *Journal of Earth Science & Climatic Change* **4**, 133.

Kim, J., Miller, N. L., Farrara, J. D. & Hong, S. Y. 2000 A seasonal precipitation and stream flow hindcast and prediction study in the western United States during the 1997/98 winter season using a dynamic downscaling system. *Journal of Hydrometeorology* **1** (4), 311–329. https://doi.org/10.1175/1525-7541(2000)001<0311:ASPASF>2.0.CO;2.

Knox, J. W., Hess, T. M., Daccache, A. & Perez Ortola, M. 2011 *What are the Projected Impacts of Climate Change on Food Crop Productivity in Africa and South Asia?* DFID Systematic Review, Final Report, p. 77. http://r4d.dfid.gov.uk/Output/186428/Default.aspx.

Kusakari, Y., Asubonteng, K. O., Jasaw, G. S., Dayour, F., Dzivenu, T., Lolig, V., Donkoh, S. A., Obeng, F. K., Gandaa, B. & Kranjac-Berisavljevic, G. 2014 Farmer-perceived effects of climate change on livelihoods in WA west district, upper west region of Ghana. *Journal of Disaster Research* **9** (4), 516–528. https://doi.org/10.20965/jdr.2014.p0516.

Legates, D. R. & McCabe, G. J. 1999 Water resources research - 1999 - legates – evaluating the use of goodness-of-fit measures in hydrologic and.pdf. *Water Resources Research* **35**, 233–241.

Legates, D. R. & Mccabe, G. J. 2013 A refined index of model performance: a rejoinder. *International Journal of Climatology* **33** (4), 1053–1056. https://doi.org/10.1002/joc.3487.

Liu, Z., Xu, Z., Charles, S. P., Fu, G. & Liu, L. 2011 Evaluation of two statistical downscaling models for daily precipitation over an arid basin in China. *International Journal of Climatology* **31**. https://doi.org/10.1002/joc.2211.

Lutz, A. F., ter Maat, H. W., Biemans, H., Shrestha, A. B., Wester, P. & Immerzeel, W. W. 2016 Selecting representative climate models for climate change impact studies: an advanced envelope-based selection approach. *International Journal of Climatology* **36** (12), 3988–4005. https://doi.org/10.1002/joc.4608.

Matthew, O. J., Abiye, O. & Univeristy, O. A. 2017 Evaluation of SDSM performance in simulating rainfall and temperature over evaluation of SDSM performance in simulating rainfall and temperature over Nigeria. https://doi.org/10.9734/BJAST/2017/32536.

Meenu, R., Rehana, S. & Mujumdar, P. P. 2013 Assessment of hydrologic impacts of climate change in Tunga-Bhadra river basin, India with HEC-HMS and SDSM. *Hydrological Processes* **27** (11), 1572–1589. https://doi.org/10.1002/hyp.9220.

Mohorji, A. M., Şen, Z. & Almazroui, M. 2017 Trend analyses revision and global monthly temperature innovative multi-duration analysis. *Earth Systems and Environment* **1** (1), 1–13. https://doi.org/10.1007/s41748-017-0014-x.

Mordey, E. K. 2021 *Woman, 65, confirmed dead in Upper West Region floods – Graphic Online*.

Najafi, R. & Hessami Kermani, M. R. 2017 Uncertainty modeling of statistical downscaling to assess climate change impacts on temperature and precipitation. *Water Resources Management* **31** (6), 1843–1858. https://doi.org/10.1007/s11269-017-1615-8.

OCHA 2007a *Special Update on Floods in West Africa – 12 Sep 2007 – Ghana | ReliefWeb*. https://reliefweb.int/report/ghana/special-update-floods-west-africa-12-sep-2007.

OCHA 2007b *Ghana: Situation Report on Floods, 11 Oct - 01 Nov 2007 – Ghana | ReliefWeb*. https://reliefweb.int/report/ghana/ghana-situation-report-floods-11-oct-01-nov-2007.

Opoku, E. K., Adjei, K. A., Gyamfi, C., Vuu, C., Appiah-Adjei, E. K., Odai, S. N. & Siabi, E. K. 2022 Quantifying and analysing water trade-offs in the water-energy-food nexus: the case of Ghana. *Water-Energy Nexus* **5**, 8–20. https://doi.org/10.1016/j.wen.2022.06.001.

Osei, M. A., Amekudzi, L. K., Wemegah, D. D., Preko, K., Gyawu, E. S. & Obiri-Danso, K. 2019 The impact of climate and land-use changes on the hydrological processes of Owabi catchment from SWAT analysis. *Journal of Hydrology: Regional Studies* **25**, June. https://doi.org/10.1016/j.ejrh.2019.100620.

Oyerindé, G. T. 2016 *Climate Change In The Niger Basin On Hydrological Properties And Functions Of Kainji Lake, West Africa*. 214.

Phuong, D. N. D., Duong, T. Q., Liem, N. D., Tram, V. N. Q., Cuong, D. K. & Loi, N. K. 2020 Projections of future climate change in the Vu Gia Thu Bon River Basin, Vietnam by using statistical downScaling model (SDSM). *Water* **12** (3), 1–17.

Sawai, N., Kobayashi, K., Takara, K., Ishikawa, H., Yokomatsu, M., Samaddar, S., Juati, A.-N. & Kranjac-Berisavljevic, G. 2014 Impact of climate change on river flows in the Black Volta River. *Journal of Disaster Research* **9** (4), 432–442. https://doi.org/10.20965/jdr.2014.p0432.

Sekyi-annan, E., Gaisie, E., Issaka, R. N. & Quansah, G. W. 2021 Estimating soil loss for sustainable crop production in the semi-deciduous forest zone of Ghana. https://doi.org/10.3389/fsufs.2021.674816.

Semenov, M. A. & Barrow, E. M. 1997 Costs of secondary parasitism in the facultative hyperparasitoid Pachycrepoideus dubius: does host size matter? *Entomologia Experimentalis et Applicata* **103** (3), 239–248. https://doi.org/10.1023/A.

Şen, Z. 2012 Innovative trend analysis methodology. *Journal of Hydrologic Engineering* **17** (9), 1042–1046. https://doi.org/10.1061/(asce)he.1943-5584.0000556.

Siabi, E. K., Kabobah, A. T., Akpoti, K., Anornu, G. K., Amo-Boateng, M. & Nyantakyi, E. K. 2021 Statistical downscaling of global circulation models to assess future climate changes in the Black Volta basin of Ghana. *Environmental Challenges* **5**, 100299. https://doi.org/10.1016/j.envc.2021.100299.

Smit, B. & Wandel, J. 2006 Adaptation, adaptive capacity and vulnerability. *Global Environmental Change* **16** (3), 282–292. https://doi.org/10.1016/j.gloenvcha.2006.03.008.

Tarek, A. S., Alaa, M. A. & Abdallah, M. K. 2016 Study the impact of climate change on maximum and minimum temperature over alexandria, egypt using Statistical DownScaling Model (SDSM). *Global Journal of Advanced Research* **8**, 694–712.

Tavakol-Davani, H., Nasseri, M. & Zahraie, B. 2013 Improved statistical downscaling of daily precipitation using SDSM platform and data-mining methods. *International Journal of Climatology* **33** (11), 2561–2578. https://doi.org/10.1002/joc.3611.

Taylor, K. E. 2001 Summarizing multiple aspects of model performance in a single diagram. *Journal of Geophysical Research: Atmospheres* **106**, 7183–7192.

Tryhorn, L. & Degaetano, A. 2011 A comparison of techniques for downscaling extreme precipitation over the Northeastern United States. *International Journal of Climatology* **31** (13), 1975–1989. https://doi.org/10.1002/joc.2208.

UN 2023 *THE 17 GOALS | Sustainable Development*. Department of Economic and Social Affairs Sustainable Development.

van Vuuren, D. P., Edmonds, J. A., Kainuma, M., Riahi, K. & Weyant, J. 2011 A special issue on the RCPs. *Climatic Change* **109** (1), 1–4. https://doi.org/10.1007/S10584-011-0157-Y.

Wilby, R. L. & Dawson, C. W. 2007 *SDSM 4.2-A Decision Support Tool for the Assessment of Regional Climate Change Impacts, Version 4.2 User Manual*. Lancaster University: Lancaster/Environment Agency of England and Wales, Leicestershire, pp. 1–94.

Wilby, R. L., Dawson, C. W., Murphy, C., O'Connor, P. & Hawkins, E. 2014 The statistical downScaling model -decision centric (SDSM-DC): conceptual basis and applications. *Climate Research* **61** (3), 251–268. https://doi.org/10.3354/cr01254.

Willmott, C. J., Matsuura, K. & Robeson, S. M. 2009 Ambiguities inherent in sums-of-squares-based error statistics. *Atmospheric Environment* **43** (3), 749–752. https://doi.org/10.1016/j.atmosenv.2008.10.005.

Willmott, C. J., Robeson, S. M., Matsuura, K. & Ficklin, D. L. 2015 Assessment of three dimensionless measures of model performance. *Environmental Modelling and Software* **73**, 167–174. https://doi.org/10.1016/j.envsoft.2015.08.012.

Yang, C., Wang, N. & Wang, S. 2017 A comparison of three predictor selection methods for statistical downscaling. *International Journal of Climatology* **37** (3), 1238–1249. https://doi.org/10.1002/joc.4772.

Yira, Y., Diekkrüger, B., Steup, G. & Bossa, A. 2016 Impact of climate change on water resources in a tropical West African catchment using an ensemble of climate simulations. *Hydrology and Earth System Sciences Discussions* 1–37. https://doi.org/10.5194/hess-2016-387.

First received 19 September 2022; accepted in revised form 30 January 2023. Available online 9 February 2023